Characterizing~~-~~ geologic and climatic controls on rockfall hazards using an inventory and integrated kinematic and runout model ~~with an integrated kinematic analysis and runout model~~: Skagway, Alaska, USA

Ian D. Wachino[1], Joshua J. Roering[1], Reuben Cash[2], and Annette I. Patton[3, 4]

[1]Department of Earth Sciences, University of Oregon, Eugene, OR, 97403, USA
[2]Environmental Department, Skagway Traditional Council, Skagway, AK, 99840, USA
[3]Sitka Sound Science Center, Sitka, AK, 99835, USA
[4]College of Forestry, Oregon State University, Corvallis, OR, 97331, USA

Corresponding author: Joshua J. Roering (jroering@uoregon.edu)

Abstract

Rockfall is common in steep terrain and poses a hazard to nearby communities. While rockfall triggering mechanisms are highly variable and difficult to quantify, the susceptibility of rock slopes to planar, wedge, or toppling failure can be readily assessed using kinematic analysis. As such, valley slopes with favourable joint orientations exhibit high rockfall susceptibility although the potential for rockfall runout to impact infrastructure and public safety depends on the morphology of downslope terrain. Integrating rockfall susceptibility and runout models with maps of talus deposits accumulated from past rockfall events is an effective combination of tools to inform mitigation but can be difficult to accomplish across extensive areas. Here, we combine these methods with a ~~a historic~~ rockfall inventory spanning 2005 to 2022 to assess geologic and climate controls on rockfall ~~hazard~~ activity in the steep and forested postglacial valleys proximal to Skagway, Alaska~~K~~, where recent rockfall activity has imperilled public safety, infrastructure, and tourism. The inventory reveals rockfall activity throughout the year with peak activity in early spring that coincides with a rapid rise in minimum daily temperatures. Our field investigations identified two steeply dipping orthogonal joint sets that favour toppling failure along NW-facing hillslopes in the lower Skagway River valley as well as the NW-facing valleys that bound nearby Dyea Bay and Nahku Bay. We used new and existing lidar data and 405~~>300~~ field-derived joint orientations to inform a kinematic toppling failure model ~~that identifies likely zones of rock topplingthat identifies. The predicted~~ source zones ~~are positioned~~ upslope of abundant talus slopes that we mapped from field observations and lidar analyses. ~~Along the prominent ridgeline on the eastern margin of Skagway, we used~~We coupled the source zones with RAMMS:Rockfall to ~~model~~ simulate ~~nearly~~ ~~200,000~~197,800 rockfall runout events for ~~four~~ scenarios ~~that account for~~with varying ~~variations in clast~~ block size and ground cover. The runout predictions highlight ~~distinct~~ zones of low and high rockfall ~~-~~propagation ~~hazard~~ susceptibility ~~along the ridgeline~~ that ~~result from changes in hillslope morphology~~ is negatively correlated with hillslope roughness which

results from ~~set by~~ the combined influence of joint orientations that generate bedrock benches and the spatial pattern of glacial erosion. High-hazard segments of the ridgeline exhibit distinct bedrock ~~escarpments~~ cliffs and slope-spanning talus slopes that result from the accumulation of rockfall activity over millennia. Taken together, our findings illustrate past controls on rockfall location and timing ~~Our findings reveal controls on past and future rockfall activity and can be used~~ to inform mitigative measures.

1 Introduction

In steep, rocky landscapes, the detachment and downslope movement of discrete rock fragments (i.e., rockfall) can occur frequently and poses a significant hazard to proximal communities and infrastructure (Hungr et al., 2014). Rockfall activity has been attributed to an array of highly disparate conditioning and triggering processes, including precipitation, frost weathering, insolation, seismic activity, and slope modification (Collins and Stock, 2016; Rosser and Massey, 2022). In Yosemite Valley, California~~A~~, for example, rockfall triggers include rainfall events, snow melt, and freeze-thaw action that can increase pressure along joints (Stock et al., 2011; Wieczorek and Jäger, 1996). Furthermore, rockfalls in Yosemite Valley may also be triggered on warm summer days by cyclic solar heating, which can propagate exfoliation fractures and lead to detachment (Collins and Stock, 2016). In the European Alps, warming and permafrost degradation have been implicated in significant increases in rockfall activity (Allen and Huggel, 2013; Bajni et al., 2021; Bodin et al., 2015; Paranunzio et al., 2015, 2016). Despite significant progress in characterizing ~~these and other~~ rockfall triggering mechanisms, prediction of rockfall timing and location has limited ability to inform warning systems (Rosser and Massey, 2022). Precursory rock deformation can signal future activity (Abellán et al., 2010; Rosser et al., 2007; Royán et al., 2014), but current methods to quantify precursor deformation across extensive areas composed of steep, high-relief surfaces are limited and oftentimes rockfall occurs without prior deformation (Abellán et al., 2011). As a result, identifying rock slopes with the propensity to generate rockfall, often referred to as rockfall source areas, is a key first step in mitigating rockfall hazards.

A wide array of methods has been proposed to assess the extent to which hillslopes are prone to rockfall activity. Delineating potential source zones (e.g., Loye et al., 2009) can be accomplished from direct observation of past events, which assumes the location of past detachments coincides with the likely location of future rockfall activity (Luckman, 1976; Matsuoka and Sakai, 1999; Rapp, 1960; Whalley, 1984). Source zones can also be inferred from distinctive evidence such as talus ~~slope~~ and scree deposits that have accumulated below cliff faces (Borella et al., 2019; Frattini et al., 2008; Moore et al., 2009; Stock and Collins, 2014). Coupled assessment of rock slope morphology and the properties of potential source zones is another common approach that uses digital elevation models (DEMs) for assessing source zones over large areas (Frattini et al., 2008; Guzzetti et al., 2003; Messenzehl et al., 2017; Samodra et al., 2016), while more data-intensive and physically-based deformation models can be used for slope-scale analyses (Matasci et al., 2018). In the absence of rock structure data, some studies (e.g., Guerriero et al., 2024) have applied morphologic criteria (e.g., slope and curvature thresholds) to DEMs

to identify anomalous rock slope protrusions that are likely to experience rockfall events (Aksoy and Ercanoglu, 2006; Frattini et al., 2008; Guzzetti et al., 2003; Marquínez et al., 2003; Sarro et al., 2024). Taken together, these studies suggest that the approach to rockfall characterization is highly dependent on the availability of data, expansiveness of the study area, and the desired level of confidence.

Because rockfall is typically localized along bedding planes, fractures, or joints, collectively referred to as discontinuities, susceptibility can also be evaluated by determining the geometry of these planes of weakness with respect to the slope and orientation of rock slopes. Kinematic analysis identifies blocks that can experience instability according to sliding, toppling, or wedge failure criteria as determined by the geometry of rock slopes and discontinuities (Fig. 1) (Bovis and Evans, 1996; Wyllie and Mah, 2004). Combining high-resolution DEMs with rock structure data can inform kinematic analyses and determine the relative likelihood of different failure modes across ~~expansive~~ extensive study areas (Grant et al., 2016; Günther, 2003; Kundu et al., 2023; Meentemeyer and Moody, 2000; Stock and Collins, 2014). Recent applications of kinematic analysis leverage lidar or photogrammetry to extract bedrock discontinuity data and test kinematic failure criteria on complex slope geometries, like overhanging rock quarries (Fanos and Pradhan, 2018; Gigli et al., 2022). Increasingly, the acquisition of discontinuity data is accomplished using automated analysis of point cloud data acquired from terrestrial laser scanning (TLS) (Matasci et al., 2018) or lidar or photogrammetry acquired from uncrewed aerial systems (UAS) (Utlu et al., 2023). These approaches are powerful but can be challenging to implement across large areas characterized by steep, rocky

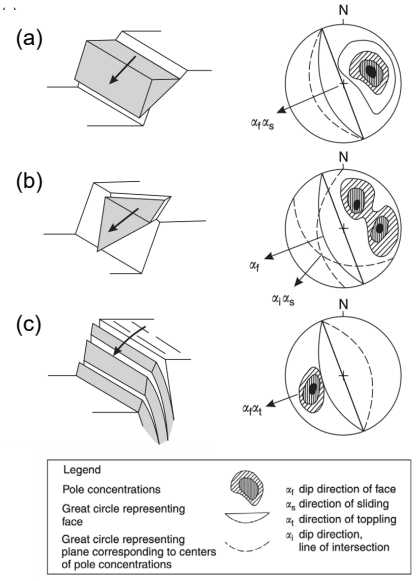

forested slopes where the details of rock structure are often obscured by vegetation. ~~As such, traditional, field-based means of bedrock structural characterization continue to be relevant.~~

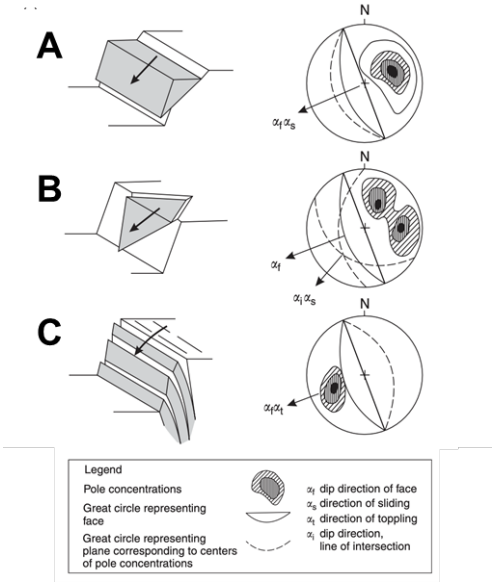

Figure 1. Schematic and corresponding stereonet representations ~~representation~~ of common rock slope failure modes: (a) planar sliding, (b) wedge, and (c) toppling. On the ~~right of each diagram are~~ stereonet plots~~s~~, ~~where the~~ the rock slope face orientation is represented by a solid black line, and poles to planar discontinuities that meet conditions for failure are shown in shaded contours. Dashed lines represent planes of these discontinuities. Modified from Wyllie and Mah (2004).

Initially, rock fragments move via creep, sliding, toppling, or falling before traveling downslope by following ballistic paths, sliding, and rolling across rocky or talus slopes until stopping when sufficient energy dissipation has occurred via impacts and/or friction (Caviezel et al., 2021). Computational rockfall runout models that account for the physics of these rockfall processes can estimate the trajectories and kinetic energy of falling rocks to determine potential downslope impacts (Dorren et al., 2007; Lu et al., 2021; Scheidl et al., 2020). Many DEM-based tools exist with a range of parameterization options to perform physically-based rockfall simulations and predict the path of rocks over complex terrain and across variable land cover (Lu et al., 2021; Moos et al., 2021). These models have been successfully employed to mitigate rockfall hazards with diversion and attenuation structures, development setbacks, signage, or other means, in a variety of settings, including mines and national parks (Guerriero et al., 2024; Klimeš et al., 2024; Stock and Collins, 2014; Stoffel et al., 2024). As a result, the

risk associated with rockfall activity~~such that rockfall risk~~ can be reduced even though accurate prediction of triggering events remains elusive (Rosser and Massey, 2022).

Although rockfall activity occurs in a wide range of geologic and climatic settings, it is particularly commonplace in post-glacial landscapes owing to glacial erosion that alters near-surface stresses, fracture density, topographic variations from glacial erosion, and changes in environmental conditions that occur in the wake of retreating glaciers (Ballantyne, 2002; Leith et al., 2014). In particular, the spatial pattern of glacial erosion can ~~follow~~ align with the fabric ~~or trend~~ of bedrock discontinuities and set up failure-prone conditions across extensive areas. As such, relatively small changes in the orientation and geometry of glacial valleys relative to the orientation of discontinuities can result in significant and systematic variations in rockfall susceptibility. Although rockfall runout susceptibility is often simulated, the terrain characteristics that govern why and where rockfall events tend to propagate long distances and pose risks downslope are seldom quantified. As a result, geologic and geomorphic controls on rockfall hazard potential are typically not well understood, which prevents us from addressing basic research and applied hypotheses such as how the magnitude and frequency of events accumulate and contribute to mountain-scale erosion and how post-glacial slope morphology affects the efficacy of mitigation efforts ~~Although it has been implied that the cumulative impact of small but frequent rockfalls in post-glacial settings can match that associated with large-scale but less frequent catastrophic or progressive rock slope failure, data are currently unavailable to rigorously test this notion~~ (Barlow et al., 2012; Corominas et al., 2014; Hales and Roering, 2007; Hungr et al., 1999; Moore et al., 2009; Rosser and Massey, 2022).

Rockfall activity is common across much of Southeast Alaska but has been particularly acute in the Municipality of Skagway, which is situated in a narrow, glacially carved valley herein referred to as the 'Skagway River valley' ~~,~~ and hosts vigorous cruise ship tourism from late spring to early fall. Indigenous knowledge of avalanches in the area has been established (Thornton, 2010) and ~~western~~ documentation of rockfall activity in Skagway by colonial settlers began in the late 1800s when gold prospecting fuelled the establishment of the town. Following decades of sporadic activity, several large rockfall events in summer 2022 impacted cruise docks along Skagway Harbor and generated renewed concern about the extent and scope of rockfall hazards in the area. In particular, the extent and timing of past rockfall activity is not well known and the susceptibility of rockfall initiation and runout in the area, and particularly along a ~5km long ridgeline that abuts the harbour, town centre, and railroad, has not been characterized. This study area affords an opportunity to explore novel approaches to combining kinematic and runout models to assess how glacial erosion and bedrock properties modulate the spatial pattern of rockfall hazard. In this contribution, we summarize a rockfall inventory~~historic~~ and geologic data that reflects the distribution and timing of past rockfall activity, document rock structure data from field observations, and synthesize new and existing lidar data from airborne and UAS platforms to inform an integrated ~~-~~kinematic analysis susceptibility and dynamic runout model ~~for Skagway and the surrounding area~~. Our findings establish the pervasive imprint of rockfall activity along slopes oriented to promote toppling failure and demonstrates how slope morphology determines

rockfall propagation susceptibility. We highlight how the pattern of glacial erosion resulted in substantial rockfall erosion and cliff retreat along favourably oriented slopes while unfavourably oriented slopes experienced minimal modification since glacial retreat. Our integrated mapping and modelling approach~~coupled modeling reveals reveal high variability in potential impacts which can inform mitigation efforts~~suggests that postglacial feedbacks between rock structure and hillslope evolution can generate strong variability in potential rockfall impacts and thus inform current mitigation efforts and anticipate future needs. ~~.~~

2 Study area: Skagway, SE Alaska

2.1. Geology and glacial history

Near the northern extent of the Alaska P~~p~~anhandle, Skagway is situated in the Taiya Inlet atop deltaic and fluvial deposits near the outlet of a deep fjord (Fig. 2). The surrounding terrain is steep and rugged, composed of Tertiary granodiorite of the Coast Range Batholith, a belt of plutonic and metamorphic rocks that extends to northern Washington (Yehle and Lemke, 1972). Deformation in southeastern Alaska and southwest Yukon is governed by the subduction and translation of the Pacific-Yakutat plates relative to the North American plate in the St. Elias region (Biegel et al., 2024). The Eastern Denali Fault and the Chatham strait fault lineaments, both strike-slip fault systems, meet just south of Skagway (Choi et al., 2021). Deformation associated with these structures appears to impart a significant influence on the orientation of glacial valleys, as fjords in the area tend to be linear, striking north and northeasterly (Yehle and Lemke, 1972). A dam reconnaissance study focused on West Creek, a drainage just 9 km northwest of Skagway, identified three joint sets in the granodiorite bedrock ~~(Fig. 3c)~~, including two abundant sets with northeast-strike and vertical or steep dips to the south, and one less abundant set with northwest-strike and a consistent vertical dip (Callahan and Wayland, 1965). That studye ~~authors~~ also noted the coincident orientation of topographic lineations in the area and the strike of joints interpreted to be splays from the Chatham strait lineament, which is related to the nearly 3,000-km long Denali fault system. Spacing between the joints is variable, ranging from 1 to 4 meters, and the joints do not exhibit slickensides or cataclastic fabric (Fig. 3a~~-c,b~~). Sheeting joints in granodiorite observed near the tops of glaciated ridges are slightly curved or irregular, tend to parallel the ground surface, and spaced from 1 to 2 meters apart at the surface. Regional studies of glacial history imply that the most recent episode of major glacial retreat and valley exposure in Skagway occurred 10 to 12kya (Baichtal et al., 2021; Menounos et al., 2017) and icefields persist today in nearby inland valleys. The steep slopes around Skagway are generally devoid of glacial till owing to post-retreat erosion and deposition in valley floors in the form of alluvial fans and colluvial deposits.

Formatted: Font: Bold

Formatted: Font: Bold

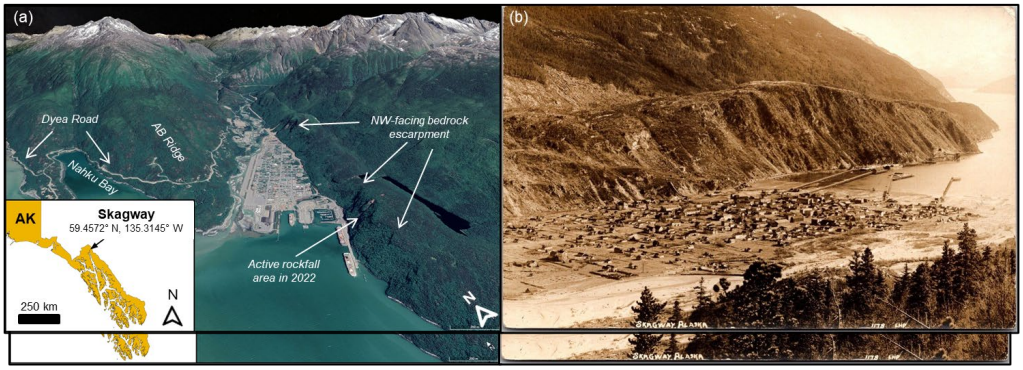

Figure 2. Study area. (a) Oblique view looking N-NE into Skagway River valley, Alaska. Note active rockfall along the NW-facing ridgeline and escarpment above the harbour and cruise ship docks. Use of Google Earth ©2025 permitted for non-~~commerical~~commercial use. (b) Oblique view from AB Ridge looking SE across Skagway towards the NW-facing ridgeline and escarpment. This undated and uncredited historic image ~~(Wright et al., 2021)~~ postdates the late 1890s construction of the current Skagway City Hall and Museum (photo provided by A. Beierly). ~~.~~ Local steep cliff faces with fresh bedrock exposure signify active rockfall. Note the lack of vegetation and the sharp bedrock escarpment along the crest of the ~~ridgline~~ridgeline and the abundance of active talus slopes that connect to the harbour.

Formatted: Correspondence

Regional studies of glacial history imply that the most recent episode of major glacial retreat and valley exposure in

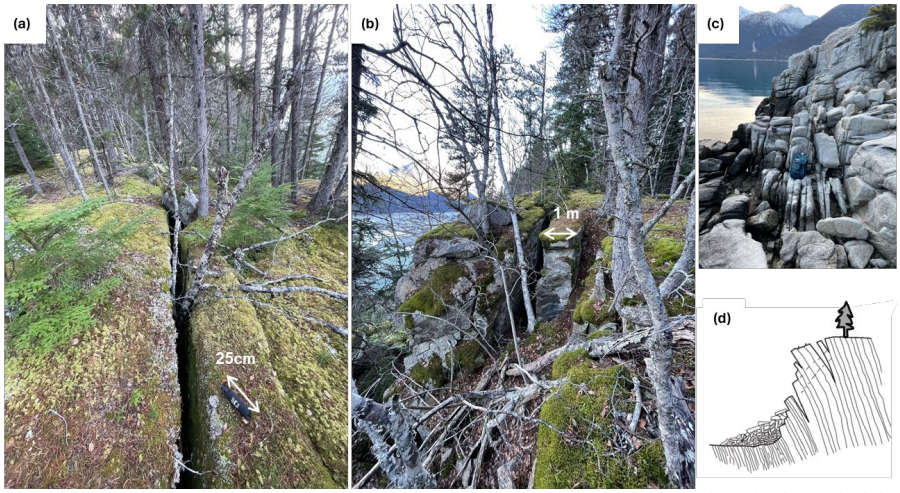

Skagway occurred 10 to 12kya (Baichtal et al., 2021; Menounos et al., 2017) and icefields persist today in nearby inland valleys. The steep slopes around Skagway are generally devoid of glacial till owing to post-retreat erosion and deposition in valley floors in the form of alluvial fans and colluvial deposits.

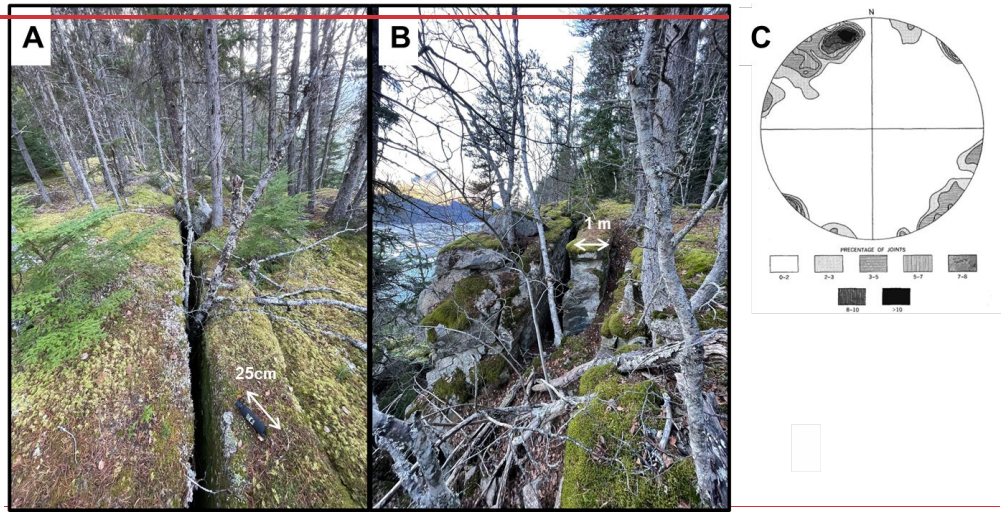

Figure 3. Images (a, ~~) and (~~b) of open joints and incipient toppling along the bedrock escarpment on the NW-facing ridgeline above Skagway Harbor. ~~Equal-area, lower hemisphere stereonet with 1% area contours of 60 joints measured near Dyea, west of Skagway. (~~c) Image of joint orientations along shore of Nahku Bay. (d) Schematic of toppling prone hillside with opening joints and talus accumulation modified from Wyllie and Mah (2004). Photos a, b, and c ~~in a and b~~ by Ian ~~Madin~~ Wachino and Josh Roering. ~~Modified from Callahan and Wayland, 1965. See Fig. 4 for location.~~

2.2. Climate and vegetation

Currently, Skagway experiences a subarctic maritime climate, characterized by cool summers and cold, snowy winters. C ~~and c~~urrent average summer temperatures range from 10 to 21°C, with occasional rainfall, and winter temperatures range from -12 to -1°C, with heavy snowfall, and freezing conditions (Western Regional Climate Center, 2025). High winds that funnel up the Taiya Inlet are common and for decades it was reported that Skagway's name originated from Lingít ~~Tlingit~~ words describing north winds (Thornton, 2010) although recent research concludes that the name derives from a contraction of 'Áa Wushigagu Ye', which translates as "the Place with Solid Core Trees" (X. Twitchell, pers. comm, 2024). Compared to other areas in SE Alaska, Skagway receives relatively low annual precipitation (mean annual precipitation is 1.1m) owing to the rain shadow imposed by the bounding coastal ranges to the south (Daly et al., 2018)~~(Western Regional Climate Center, 2025)~~. Atmospheric rivers account for nearly 70% of annual rainfall in Skagway and intense precipitation associated with these phenomena occur with highest frequency and intensity from August to October (Nash et al., 2024). Skagway hosts a coastal rainforest of spruce (*Picea sitchensis*), pine (*Pius contorta*), and cedar (*Chamaecyparis nootkatensis*) trees with dense underbrush at low elevations (under 1,000m above sea level) and high-alpine tundra above tree line (Harris and Farr, 1974). Historical photographs and descriptions suggest that forests covering the slopes perched above Skagway Harbor and township were disturbed ~~timber~~ through timber harvest and burning in the early 1900s (Wright et al., 2021).

2.3. Historic rockfall activity

Early Western descriptions of rockfall activity in Skagway tend to focus on impacts to the harbour and railroad, including a series of events in 1901 that recorded burial of the tracks near the approach to the wharf (The Daily Alaskan, 1901). The location of this event coincides with the steep rocky slopes above Skagway Harbor, which have generated numerous rockfalls since that account (Fig. 2). A study of geologic hazards in Skagway noted the striking linearity of N- and NE-oriented fjords and valleys and ~~s and~~ identified abundant actively eroding bedrock escarpments on a NW-facing ridgeline ~~that runs along the eastern margin of Skagway~~that coincides ~~that coincides~~ with a zone of historic rockfall activity adjacent to the township and harbour (Yehle and Lemke, 1972). Downslope of these escarpments are colluvial deposits, consisting of landslide deposits, including talus from historic rockfall events. The abundance and extent of these deposits implies significant slope adjustment and retreat since glacial retreat and the relative activity of the deposits is ~~based~~ reflected by~~on~~ the relative abundance ~~or absence~~ of vegetation cover (Ruffner and Abrams, 1998; van Steijn, 2002). Across the valley on

Formatted: Font: Bold

Formatted: Font: Italic

Formatted: Font: Italic

Formatted: Font: Italic

Formatted: English (United States)

Formatted: Font: Bold

the western side of Skagway, these talus deposits are much less prevalent, and the Yehle and Lemke (1975) maps do not indicate the presence of erosional escarpments.

Rockfall hazard mitigation in the area is currently focused on the active rockfall source areas above the cruise ship dock in Skagway Harbor. On June 23, 2022, rocks detached from the eastern ridgeline and impacted the cruise ship dock where pedestrian traffic is frequent (Munson, 2022b). Two more rockfall events originating in the rocky slopes above the harbour followed in rapid succession on August 3 and 5, 2022 (Munson, 2022a).

~~Rockfall hazard mitigation in the area is currently focused on the active rockfall source areas above the cruise ship dock in Skagway Harbor.~~ Engineering efforts have been completed, which include wrapping rock mesh covers over source areas, installing attenuator nets to block falling rocks, and scaling loose rocks (Brennan and Whistler, 2022). Instrumentation has been installed to monitor the source area, including extensometers installed at the top of the slope, which show that movement in the slide mass has increased from 4 cm per year to 6.5 cm per year as of 2022 (Brennan and Whistler, 2022). Notably, the small section of rocky slopes above Skagway's cruise ship dock ~~, where the engineered mitigation and monitoring efforts are focused,~~ is a small fraction of the roughly 5-km long stretch of ridgeline that borders the eastern margin of Skagway. Rocky escarpments and talus deposits have been noted along the entire ridge (Yehle and Lemke, 1972), including the "Cemetery Slide", a rockfall source area and runout zone stripped of vegetation by falling debris, which is similar to the active source areas above the cruise ship dock. Although these zones of localized activity are well known, ~~the~~ forest cover obscures the geologic and topographic signature of past rockfall activity along the remainder of the ridge such that the pattern of relative susceptibility and runout remains ambiguous.

3 Methods

3.1. Overview

Motivated by renewed rockfall activity, this study seeks to identify areas susceptible to rockfall initiation and runout within the steep, post-glacial valleys around Skagway. Our analysis extends to the west of Skagway along Dyea Road to the Taiya River, which hosts the Lingít ~~Tlingit~~ settlement of Dyea and the Chilkoot Trailhead~~, which is~~ . Dyea Road is a well-travelled corridor that also provides the opportunity to test our methodology across a wider range of topographic and structural configurations (Fig. 4). ~~The components of our analysis include a historical rockfall inventory, synthesis of new and existing lidar data, geomorphic and structural mapping, kinematic analysis of rockfall susceptibility, and rockfall runout modelling.~~

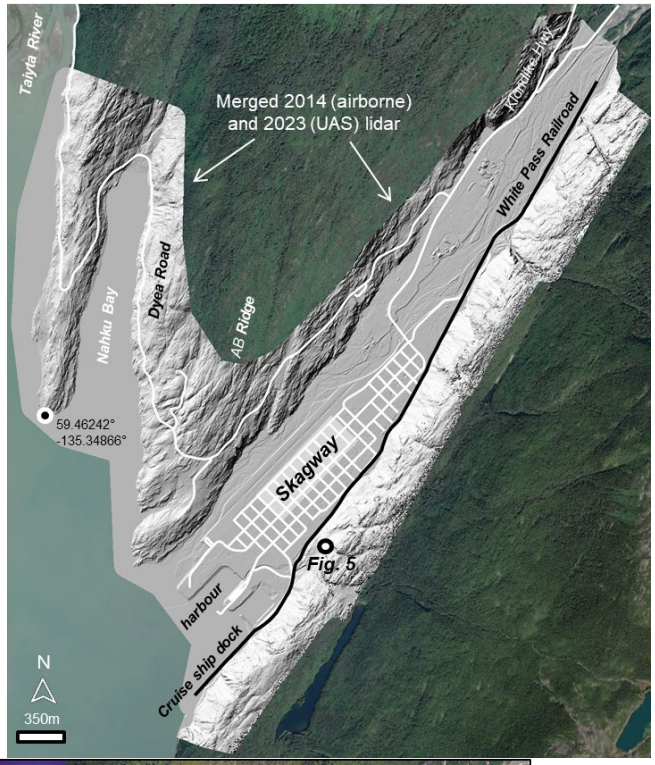
Taiyta River
Merged 2014 (airborne)
and 2023 (UAS) lidar
Klondike River
White Pass Railroad
Dyea Road
Nahku Bay
AB Ridge
59.46242°
-135.34866°
Skagway
Fig. 5
harbour
Cruise ship dock
N
350m

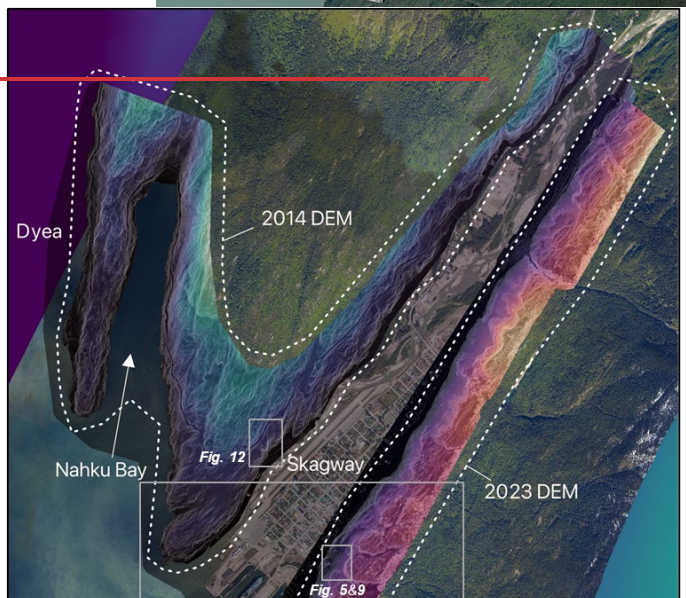
Dyea
2014 DEM
Nahku Bay
Fig. 12
Skagway
2023 DEM
Fig. 5&9

Figure 4: Location map of Skagwayy River valley, Nahku Bay, and Dyea Road showing a merged hillshade image of the 2014 airborne survey and 2023 UAS lidar bare earth dataDEM acquired for this study. White lines denote roads and the thick black line denotes a section of White Pass Railroad and cruise ship dock used for our rockfall runout susceptibility analyses. The 2023 UAS lidar data was acquired along the ridge southeast of the railroad while the 2014 airborne lidar accounted for the remainder of the study area imagery shown here. The dashed lines demarcate the areas analyzed in this study. Gray boxes denote the extent of other figures.Location of Figure 5 is shown by black/white filled dot. Background image from USGS NAIP (National Agriculture Imagery Program).

3.2 Rockfall inventory

To investigate controls on rockfall timing, wWe searched newspaper articles (primarily the Skagway News) and public announcements that describe the location and timing of rockfall events since August 26, 2017, which marks the beginning of rockfall mitigation efforts along the Skagway Harbor. In addition, we accessed data generated for rockfall events between 2005 and 2022 from the GeoEvent Slope Stability Database generated by the Alaska Department of Transportation & Public Facilities (AKDOT&PF) Geotechnical Asset Management Program (Thompson, 2017). This database features includesdetails from AKDOT&PF maintenance and operations reports, including the location, date, event type (e.g., debris flows, rockfalls, landslides, snow avalanches, flooding), relative magnitude, and cost, of geologic slope processesevents that impact the Alaska highway system. Notably, this database does not include information for activity along the White Pass Railroad that abuts the rockfall-prone ridgeline along the eastern margin of Skagway. Nonetheless, it includes 866 rockfall event reports along segments of Skagway-Dyea Road and Klondike Highway within our study area (Figure 4) that enabled us to assess climatic controls on rockfall activity. We aggregated rockfall events according to Julian day to investigate seasonal trends in activity over the 17-yr record. For climate context and comparison, we accessed Skagway Airport (PAGY) mean daily rainfall and mean daily maximum and minimum temperature data for 2005 to 2025 (Horel et al., 2002).

3.3 High-resolution topography: Airborne and UAS lidar

Our analysis used two sources of lidar data to inform geomorphic and bedrock mapping, kinematic analysis, and runout modelling. One We used a 2014 airborne lidar dataset DEM acquired in 2014 with an average ground classified point density of 4.6 m^{-2} is available fromacquired by the Alaska Department of Geological and Geophysical Surveys (DGGS Staff, 2013) and which includes low-elevation terrain in the Skagway River valley, Nahku Bay, and part of Dyea valley (Macpherson et al., 2014). Because this lidar acquisition does not span a significant portion of Skagway's rockfall-prone east ridge that abuts the township and harbour, we conducted a UAS lidar survey in 2023 (Fig. 4). We acquired lidar data across the 2.3 km^2 area with peak elevations of 220 m near the cruise ship docks and 320 m near the northern extent of the ridgeline (Roering et al., 2025). For the acquisition, the NSF RAPID facility used a Trinity F90+ fixed wing drone with a Qube 240 lidar payload to fly ~120m above ground with 90% coverage overlap. The surveyed area was slightly abbreviated due to a patch of extremely steep terrain where the UAS could not be flown safely at distances sufficiently close to the ground

surface to acquire data. The UAS survey produced a point cloud containing 650 million total points with 200 million ground classified points, giving an average ground point density of 43 m^{-2}. We used the ground points to create a 1 m DEM using Cloud Compare (version 2.12.3) and combined it with the 2014 airborne lidar data to provide a ~~seamless~~ continuous lidar coverage for our analyses (Fig. 4).

3.4 Geomorphic mapping

We used field observations, historic photographs, and slope thresholds and surface texture from the combined lidar DEM to identify and map talus deposits that reflect the accumulation of rockfall deposits. These talus deposits include both forested and ~~exposed~~ unforested occurrences. To define the characteristic slope angles associated with active talus slopes we measured slope angles from 20° to 45° that coincide with mapped talus deposits along the eastern ridge. Slopes steeper than 45° tend to correspond with bedrock cliffs and outcrops, whereas slopes gentler than 20° often reflect relatively uneroded bedrock surfaces or deposits from fluvial or other mass wasting processes. The relatively smooth texture of accumulated rockfall deposits identified with hillshade and slopeshade layers (Burns and Madin, 2009) was also used to identify active talus slopes as well as bedrock cliffs or outcrops that constitute a rockfall source area. Talus deposits occur on a wide range of scales and for this analysis we focused on mapping patches of talus with area >100m^2 to ensure accuracy and highlight zones of significant activity (Fig. ~~5~~5). Specifically, we identified terrain that exhibits the relevant slope values as well as surface textures consistent with talus deposits and then mapped polygons that enclose these zones when their areas exceeded 100m^2. The polygons were often separated by bedrock outcrops, gullies, and anthropogenic features.

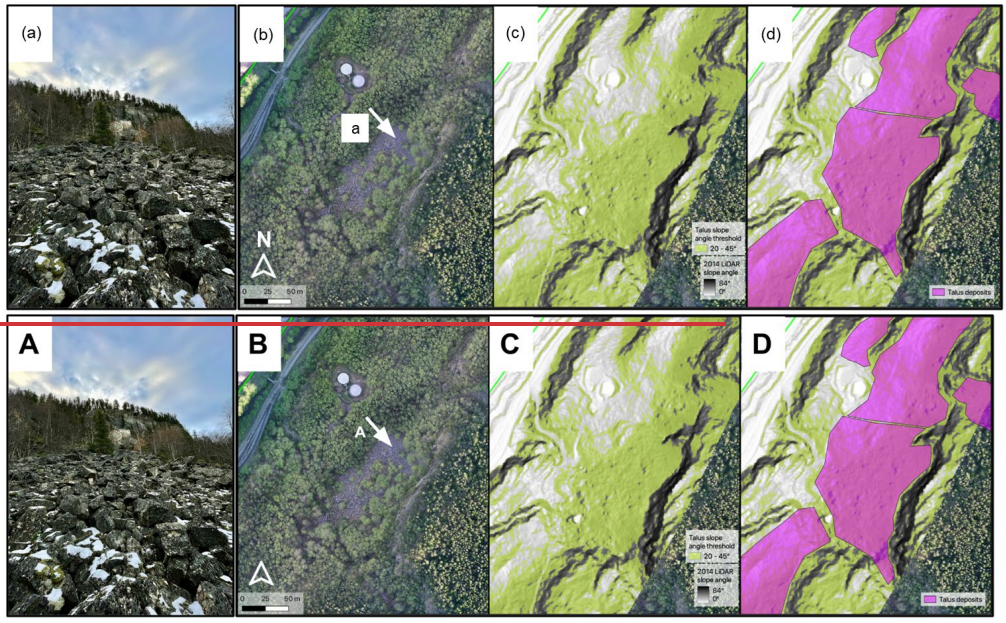

Figure 55: Field images and lidar mapping of talus mantled slopes. ~~See Fig. 4 for location.~~ (a) View looking SE along an exposed talus deposit with boulder sized ~~clasts~~ blocks at the base of a 40 m cliff known as Kirmse's Cliff (lat: 59.45251, long: -135.31147)~~on far left of image~~, (b) Aerial imagery from 2023 UAS survey showing ~~the~~ a talus deposit and bedrock cliff ~~(center left)~~, white arrow ~~represents~~ shows view direction for ~~a~~photograph location and view direction, (c) Terrain within the slope angle range of 20°-45° colored in ~~yellow~~light green, and (d) map of talus polygons (pink) generated from lidar slope shade and slope angle maps and orthoimagery. Hillshades in c and d derived from ~~DGGS~~ 2023 UAS lidar data. Background image from USGS NAIP (National Agriculture Imagery Program).

Formatted: Normal

3.5 Bedrock structure and discontinuities

To quantify the geometry of joints and discontinuities that contribute to rockfall initiation, we collected 405 structural measurements (specifically, the strike and dip of planes that define the interfaces) at ~~a range of distinct locations~~nearly 50 locations within the study area and combined them to generate a comprehensive discontinuity dataset (Kundu et al., 2023). The steep, forested, and uneven terrain surrounding Skagway limits access to outcrops and the traditional 'scanline' method

(Priest and Hudson, 1981) was untenable. Furthermore, the significant forest cover and expansiveness of the study area precluded the use of ground-based laser or SfM (structure from motion) methods for acquiring structural information. Instead, we traversed the base of outcrops as an approximation of scanlines and measured the orientation of planar surfaces expressed in the outcrop with FieldMoveClino, a digital compass-clinometer smartphone app (Oliinyk et al., 2020), which enabled rapid and accurate data acquisition. Our measurements were acquired across a wide range of locations in the study area ~~in order to~~to characterize spatial variations in discontinuity orientations. In particular, we visited outcrops along the eastern, southern, and western ~~sides~~ corners of the ~~Skagway River valley~~study area ~~as well as outcrops in secondary valleys perpendicular to these ridgelines~~ to ensure that the full range of relevant joint orientations ~~were~~ was represented (Terzaghi, 1965). We identified joint clusters by converting the strike and dip of discontinuity planes to poles on stereonet plots and used contouring to separate different clusters (Wyllie and Mah, 2004).

3.6 Kinematic analysis of rockfall susceptibility

To assess the spatial pattern of rockfall susceptibility across the study area, we adopted a kinematic analysis approach with our discontinuity data and applied criteria for planar sliding and toppling failure within our combined lidar DEM. This approach foregoes the mechanical complexity and extensive parameterization of more sophisticated analyses (e.g., Matasci et al., 2018) in order to generate results that span an extensive area. Kinematic analysis requires discontinuity data that is locally representative. Traditionally, discontinuity measurements are taken in the field, whereas many modern applications extract discontinuity orientations from high-resolution point clouds of the rock slope face (Utlu et al., 2023). Field measurements remain a reliable and relevant means to capture joint orientations (Kundu et al., 2023), especially in locales where terrestrial laser scans are not feasible due to hazardous terrain or where slope faces are obscured by vegetation. As described below, the remarkable consistency of discontinuity orientations across the study area inspired this approach and therefore we invoked the entire distribution of measured joint orientations at all locations to perform the kinematic analysis. Specifically, we applied the stability criteria for each failure mode at each pixel in the ~~combined~~ merged lidar DEM by estimating the fraction of the ~~337~~ 405 joint orientations that are predicted to be unstable given the topographic aspect and slope angle of that pixel. The failure criteria for planar and toppling failure are defined following Wyllie & Mah (2004) and described below. Essentially, this approach is equivalent to locally performing a stereonet analysis of rock slope failure across our study area and aggregating the results to identify potential rockfall failure modes ~~as well as~~and areas of high relative susceptibility. For the analysis, we used a friction angle of 40°, consistent with measured values for jointed granodiorite similar to Skagway's lithology (Alejano et al., 2019). To assess the accuracy ~~For validation~~ of our modelled rockfall susceptibility maps, we visually compared our predictions to the location of recent rockfall events in Skagway, as well as mapped bedrock cliffs and talus deposits, which serve as a proxy for prior rockfall activity (Loye et al., 2009; Stock and Collins, 2014). In addition, we compared the downslope direction of talus deposits with the aspect of topple-prone slopes to assess their relative correspondence.

Planar slides occur when the inclination of a bedrock slab exceeds the friction angle and it slides along a planar discontinuity. Toppling failures occur when discontinuities steeply dipping into the rock slope face form slabs or columns of rock that rotate forward along a fixed base (Fig. 1). Two types of toppling failures can occur that are influenced by the strength of the rock mass and the geometry of discontinuities. Flexural toppling, where slabs of rock bend forward until they break in flexure, is typical in shale and slate where orthogonal jointing is not well developed. Block toppling is common in crystalline bedrock with orthogonal joint sets, where two steeply dipping joint sets form the sides of blocks, and a third set of low angle, widely spaced joints form a basal failure plane. The active rockfall source area situated above Skagway's cruise ship dock has been described as a progressive toppling failure with a stair-stepped basal feature (Brennan and Whistler, 2022). Topple failures observed in the field are consistent with this description, which is described by the block toppling failure mechanism. As a result, our analysis focuses on block toppling and planar sliding given that ~~although we also account for planar sliding given that sporadic sliding was observed in the field. F~~ field observations and geotechnical reports do not identify wedge failures as a prevalent mechanism of rock slope instability. The challenge of implementing multiple discontinuity orientations required for wedge analyses across our entire study area also encouraged us to focus on block toppling and planar sliding ~~a potential mechanism and we opted not to include it~~ in our analyses.~~.~~

The criteria for planar, wedge, or toppling failure is based on the orientation of discontinuities and their orientation relative to the rock slope face (Wyllie and Mah, 2004). The dip direction of the discontinuity (A) and rock slope (f) is given by α_A and α_f, respectively, and the dip angle of the discontinuity and rock slope, both relative to horizontal, is given by ψ_A and ψ_f, respectively. The friction angle of the joint interfaces is given by ϕ.

Accordingly, a rock slope is susceptible to planar sliding failure along a discontinuity if the following three conditions are simultaneously met:

$$|\alpha_A - \alpha_f| < 20° \; ; \; \psi_A < \psi_f \; ; \; \psi_A > \phi \tag{1}$$

The first condition requires that the interfaces are aligned in a sufficiently similar orientation (in this case within 20°) while the second ensures that the discontinuity dip is shallower than the angle of the bedrock slope such that the discontinuity intersects or 'daylights'. The third and final condition demands that the interface slope angle exceeds the angle of friction. All three conditions must be met at a given location for planar sliding to be deemed likely.

For block toppling failure, the following two conditions must be met simultaneously:

$$\alpha_f - 20° < (\alpha_A \pm 180°) < \alpha_f + 20° \; ; \; (90° - \psi_f) + \phi < \psi_A \tag{2}$$

The first condition asserts that the discontinuity must dip into the rock slope face and be parallel, or nearly parallel (e.g., within 20°), to the dip direction of the slope face. The second condition indicates that the discontinuity dip must exceed the friction angle allowing for interlayer slip between the blocks. In our model, the maximum allowable dip direction deviation is ± 20° for both planar slide and block toppling failure. Although this value is sometimes ~~was often~~ chosen to be ± 10° for block toppling we expanded the constraint to ± 20° ~~, consistent with recent contributions~~ (Cruden, 1989; Gigli et al., 2022).

~~Kinematic analysis requires discontinuity data that is locally representative. Traditionally, discontinuity measurements are taken in the field, whereas many modern applications extract discontinuity orientations from high-resolution point clouds of the rock slope face (Utlu et al., 2023). Field measurements remain a reliable and relevant means to capture joint orientations (Kundu et al., 2023), especially in locales where terrestrial laser scans are not feasible due to hazardous terrain or where slope faces are obscured by vegetation.~~

Using equations 1 and 2, we estimated the number of joints in our field-derived dataset (n=405~~337~~) that are predicted to exhibit planar and toppling failure, respectively, for each pixel in our ~~combined~~ merged lidar DEM. Also, by simultaneously accounting for both modes of potential failure at a given location it is possible to assess the combined susceptibility to toppling and planar sliding although we do not formally account for this possibility in our analysis. Our maps of planar and toppling failure are then calculated as the percentage of joints that meet the conditions required for failure conditions at each pixel in our study area. ~~For~~ For example, a toppling failure index value of 0.21~~31~~ for a given pixel in our DEM indicates that 2~~3~~1% of the joints in our joint dataset satisfy the two conditions in equation 2. This approach provides a description of relative rockfall initiation susceptibility across our study area.

3.7 Rockfall runout modelling with RAMMS

To model potential runout paths associated with rock slopes that have high rockfall susceptibility, as determined by our kinematic analyses, we used the 3D rockfall simulation software RAMMS:Rockfall (https://ramms.ch/ramms-rockfall/) to represent the sliding, bouncing, and rolling motion of block~~rock clast~~s as well as the internal, gravitational, and contact forces of a rigid body that can translate and rotate. This model accounts for the energy balance of falling rocks and has been used extensively at a range of scales for both applied and fundamental research studies (e.g., Caviezel et al., 2021; Kleinn et al., 2024; Leine et al., 2014; Lu et al., 2019; Ringenbach et al., 2023). The primary inputs required for the RAMMS:Rockfall model include digital elevation data (i.e., DEM), the location of rockfall source areas, specification of ground cover, and the shape and size of the falling blocks.

We used our ~~combined~~ merged lidar DEM, which has a 1x1 m pixels and spans the area shown in Fig. 4. To identify potential source areas, we identified pixels in our maps of toppling susceptibility with values greater than 5%. Pixels with >5% toppling susceptibility demarcate rocky cliffs situated above our mapped talus deposits as well as areas of recent

rockfall activity in the Skagway Harbor (Fig. 5). The pixels with a >5% high toppling susceptibility were converted to polygons and only polygons with area greater than ~~25~~ 25 m^2 were retained ~~in order to~~to eliminate local high-relief features like boulders and trees that can perpetrate the signature of rockfall source zones. Rockfall source points for RAMMS modelling were randomly distributed across the resulting polygon coverages with a density of 0.~~02~~ 04 m^{-2} and a minimum point spacing of 5 m. This methodology follows convention used in other studies (Lu et al., 2021) and yielded ~~nearly~~ ~~5,000~~4,945 rockfall initiation points for each of our ~~RAMMS simulations.~~simulation scenarios.

The slopes east of Skagway are heavily forested, except in locations where falling debris has stripped vegetation, such as the cruise ship dock and at the northern extent of the eastern ridge bordering Skagway. In RAMMS, we represented forested areas as spruce alpine forests and trees were simulated in these areas using the 'dense forest' category in RAMMS, which is defined by a stem density of 600 trees per hectare with a mean diameter of 30 cm. These parameters were chosen based on our field observations and the typical density of mixed red alder coniferous stands in Southeast Alaska (Poage et al., 2007). The effect of trees in the RAMMS rockfall runout module is to attenuate energy and reduce velocity, thus constituting a significant impact on hazard potential. We mapped the distribution of trees by visually assessing the USGS NAIP imagery as well as our UAS orthoimagery. The ~~very~~ small amount of terrain (less than 5% of the study area) that exists outside these forested areas was set to the fine talus cover category in RAMMS, which reflects negligible ground cover atop relatively fine-grained talus deposits consistent with our field observations. We performed simulations with two land cover scenarios: 1) ~~and without~~ dense forest ~~forest cover~~ and 2) fine talus cover, assigned across the entire simulation area ~~in order to~~to assess the potential role of timber harvest and fire on rockfall runout and provide a conservative assessment of the hazard extent.

We estimated representative block size and shape by measuring the major axes of randomly selected blocks in exposed talus piles (Hales and Roering, 2007). To estimate representative block sizes, the intermediate axis of 74 blocks was measured from field measurements and high-resolution point clouds combined with orthoimagery. We determined the mean intermediate axis size to be 1.08 m while the 50th percentile was 0.66 m and the 95th percentile was 3.56 m. Blocks observed in the field are typically tabular and the characteristic ~~shape~~ geometry of blocks was estimated by measuring the long, intermediate, and short axes of 10 blocks with sufficient exposure to allow measurement using our UAS-derived point clouds. ~~The block dimensions were measured and w~~We applied the ~~resulting~~ characteristic aspect ratio to the 50th percentile and 95th percentile intermediate axis values from our ~~block size~~ measurements. The dimensions of the resulting rocks used in the simulation were 0.94 m x 0.66 m x 0.37 m (medium, 50th percentile), and 5.10 m x 3.56 m x 1.99 m (large, 95th percentile), which represent moderate and large ~~clast~~ block sizes, respectively. Given the tendency for large ~~clasts~~ blocks to travel longer distances, our 95th percentile blocks are intended to reflect the conservative (or long runout) scenario (Statham, 1976). For these simulations, we assumed rock density of 2,700 kg m^{-3}.

To simulate the range of potential rockfall impacts, we focused on four scenarios for RAMMS simulation with the following parameterizations: 1) 50th percentile ~~clasts~~ block with fine ~~no forest~~talus cover, 2) 50th percentile ~~clasts~~ block with dense forest, 3) 95th percentile ~~clasts~~ blocks with fine ~~no forest~~ talus cover, and 4) 50th percentile ~~clasts~~ block with dense forest. To account for the stochastic nature of rockfall release, we used RAMMS to select 1 of 10 randomly chosen ~~rock clast~~ block orientations to be released at each source point, yielding ~~nearly 50,000~~49,450 individual rockfall runout paths ~~in~~ for each of the four ~~simulations~~scenarios. Our results presented here focus on the two end-member scenarios (50th percentile with dense forest cover and 95th percentile with fine-grained talus over) to illustrate the range of rockfall behaviour.

For our runout analysis, we focused on the eastern NW-facing ridgeline of the Skagway River valley to assess potential~~given the need to assess~~ impacts to the harbour and township. ~~Because each simulated runout event results in an individual rockfall path, it can be difficult to effectively visualize the cumulative pattern of predicted runout~~We used an array of analyses to investigate rockfall runout patterns and topographic controls on the runout behaviour. First, t~~T~~o identify terrain with high likelihood of rockfall runout we used RAMMS to ~~count~~ calculate the number of rockfall events that traversed each pixel in our model domain for each of the ~~four~~ scenarios. As such, the cumulative number of rockfall passages at each pixel accounts for both the abundance of upslope source areas as well as the tendency for topography to steer or direct rockfall into particular pathways. Second, ~~In addition,~~ we used RAMMS to create a "digital" boundary (or barrier) coincident with the railroad tracks along the base of the ridgeline to record ~~the number and kinetic energy of modelled~~ rockfalls that bypass the boundary and have the potential to impact the harbour and township. Third, to estimate how topographic properties moderate rockfall runout, we calculated local slope and terrain roughness across the simulation domain. Roughness was calculated as the standard deviation of local slope values within a 5-m radius window. This approach has been successfully used to differentiate the kinematics and age of landslide deposits (Booth et al., 2017; LaHusen et al., 2020) and in this case, we choose the 5-m scale to be consistent with the scale of blocks, fractures, and bedrock landforms. Finally, we generated a 5.4-km long transect coincident with the railroad within our simulation domain to quantify along-ridge variations in rockfall passages, upslope source areas, slope angle, and terrain roughness.

4 Results

4.1 Rockfall inventory

~~Descriptions of rockfall events before 2005 can be found in newspaper articles dating back over a century, although we focus on recent events in this contribution. We identified 11 reported rockfall events reported in the Skagway News since 2017 (Table 1). These reports tended to reflect sporadic rockfalls along Dyea Road as well as activity in 2022 abutting Skagway Harbor on the eastern ridgeline. Many reports are recorded in the police blotter section of the Skagway News, but the timing and location of these events is sometimes unclear and those cases were not included in our rockfall inventory.~~ The AKDOT&PF ~~GeoEvent~~ database includes ~~536~~ 866 reports of rockfall-related maintenance and operation activities ~~in our~~

Formatted: Superscript

Formatted: Superscript

~~study area~~ along the 10.3-km long segment of Skagway-Dyea and Klondike Hwy within our study area between 2005 and 2022 (Fig. 6,7). ~~Notably, this database does not include events along the eastern ridgeline in Skagway because those events do not impact the state highway system. Rather, the vast majority (>415) of the AKDOT reports originate from the NW-facing sections of Dyea Road west of Skagway. Among those events, 7 resulted in road closures that lasted 3 days or longer in March 2012, October 2012, January 2014, March 2015, February 2016, September 2016, and December 2020.~~ This implies an average rockfall frequency of 50 events per year, although this value is an overestimate because some of the reports are redundant given that multiple days are reported in response to a single event. Among the events, 7 resulted in road closures that lasted 3 days or longer in March 2012, October 2012, January 2014, March 2015, February 2016, September 2016, and December 2020.

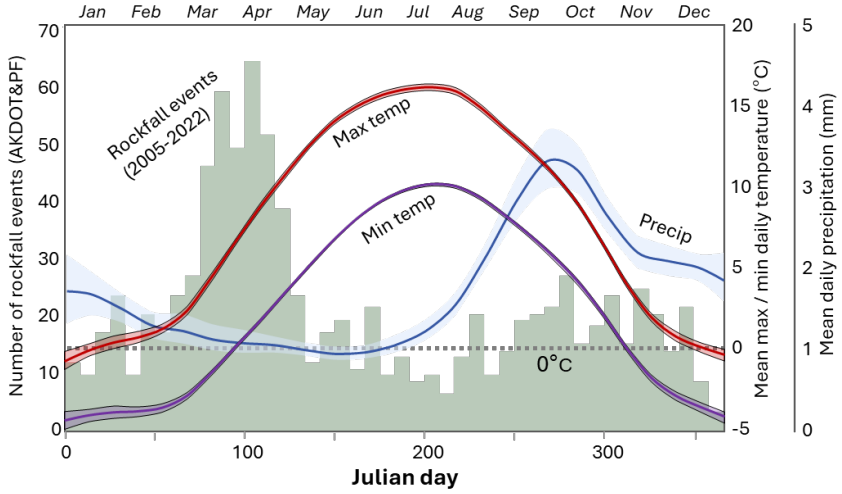

Figure 6. Analysis of seasonal variation in rockfall activity and climate variables from the AKDOT&PF geoevent database (2005-2022) and daily mean precipitation and daily maximum and minimum temperature from the Skagway Airport (PAGY) for the period 2005-2025. The number of rockfall events (green bars) exhibits seasonal variations that don't obviously align with precipitation (blue) although maximum temperature (red) and minimum temperature (purple) increase significantly during the typical period of rockfall activity in March and April. The horizontal dashed grey line represents freezing. The confidence intervals for the climate data represent standard error of mean values over the period of record.

~~Table 1: Rockfall events reported in the Skagway News since 2017~~

Event date	Event time (local)	Pre-event 24-hr rainfall total (inches)	Location
9-Oct-2023	n/a	0.63	East Dyea Valley
7-Oct-2023	n/a	1.46	Eas Nahku Bay
18-May-2023	6:17pm	0	North Slide
29-Sept-2022	3:57pm	0.50	East Nahku Bay
5-Aug-2022	n/a	0.04	North Slide
3-Aug-2022	5:00pm	0.02	North Slide
23-Jun-2022	7:30am	Trace	South Slide
2-Dec-2020	12:23pm	3.24	East Nahku Bay
5-Sept-2017	5:30am	0.76	North Slide
5-Sept-2017	3:00am	1.05	North Slide
26-Aug-2017	6:30am	0.55	North Slide

According to our analysis, rockfall events peak in late March and April, occurring at a pace that is 4x greater than the remainder of the year (Fig. 6). This substantial uptick in activity corresponds with a seasonal increase in daily temperatures, particularly when the minimum daily temperature exceeds zero. This implies that thawing of frozen rock slopes promotes the destabilization of blocks through the loss of tensile strength and increases in pore pressure from melting ice and snow. In the fall, increased daily rainfall associated with atmospheric rivers with a detectable but small increase in activity. The mid-summer period of warm temperatures and dry conditions corresponds with the least active period.

Rockfall events reported in the newspaper and AKDOT database occur sporadically throughout the year with most activity in the summer and fall months. Some notable high impact rockfall events correspond with intense rainfall events although most events do not coincide with an obvious climatic trigger. , Rockfall activity oninclucding December 2, 2020, was when widespread events were preceded by over 3 inches of rainfall in the previous 24 hours. By contrast, a May 2023 event, which we observed in the field, initiated on a clear, sunny day with no precipitation in the 24 hours leading up to the event. In addition, the August 2022 events that impacted Skagway Harbor were not preceded by notable rainfall. Thus, while precipitation plays a role in initiating some rockfall events in Skagway other triggers maybe relevant making prediction difficult.

4.2 Geomorphic mapping

The morphology of glaciated valleys around Skagway is variable owing to bedrock structure, differential glacial erosion, and post-glacial landscape evolution (Fig. 4). These factors generate systematic variations in the abundance of bedrock cliffs that serve as rockfall source areas as well as long, steep slopes that facilitate long rockfall runout. On the east side of the lower Skagway River valley, our lidar DEM and field observations reveal a distinct northwest-facing bedrock escarpment that runs parallel just below the crest of the ridgeline (Fig. 71, 6). This feature is particularly distinct above the cruise ship dock, where the ridgeline has high relief compared with sections to the north that abut the township. A similar high-relief escarpment also emerges on the same ridgeline near the northern extent of the township. Below these bedrock escarpments, we observe abundant talus deposits that extend continuously downslope to the base of the ridgeline and the valley floor (Fig. 76). An undated historic photograph which postdates the 1899 construction of the current Museum and City Hall depicts the

eastern ridgeline in a state of minimal forest cover such that the escarpment and talus slopes above the harbour are clearly visible (Fig. 2b). These observations imply substantial post-glacial erosion through lateral (southeastward) retreat of the ridgeline as talus slopes convey bedrock downslope creating long and relatively smooth pathways for rockfall runout. In Figure 2b~~On that image~~, the ridge~~line slopes just north (~~on the left side of the image~~)~~ exhibits gentler slope angles (<20°) and a benchy morphology which implies less extensive post-glacial erosion and slope modification via rockfalls ~~(Fig. 2b)~~. Atop the ridge~~line~~ and east of the escarpment, the ridgeline contains abundant evidence of unmodified glacial erosion features (Figure 4).

By contrast, t~~T~~he west side of the ~~lower~~ Skagway River valley has a very different morphology, in that it lacks a distinct escarpment and instead exhibits consistent and gradual slopes that imply minimal post-glacial modification. Locally, we observe vertical cliffs along the Skagway River~~. Otherwise~~ but otherwise~~,~~ the ~~topography on the~~ west side of the ~~lower~~ Skagway River valley ~~primarily~~ consists of gentle rock slopes that form prominent ridges ~~that~~ and parallel the strike of the valley. We observe a similar pattern of bedrock escarpments and talus deposits along the NW-facing~~northwest-facing~~ slopes of two parallel ridgelines between Skagway and ~~Dyea~~ the Taiya River (Fig. ~~6~~7).

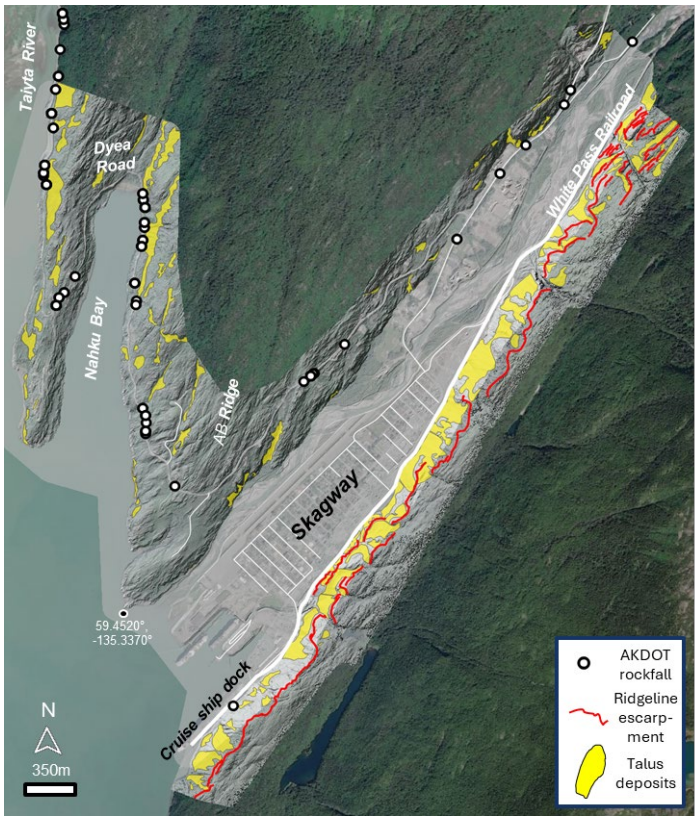
Taiyta River
Dyea Road
Nahku Bay
AB Ridge
Skagway
White Pass Railroad
59.4520°,
-135.3370°
Cruise ship dock
N
350m
AKDOT rockfall
Ridgeline escarp-ment
Talus deposits

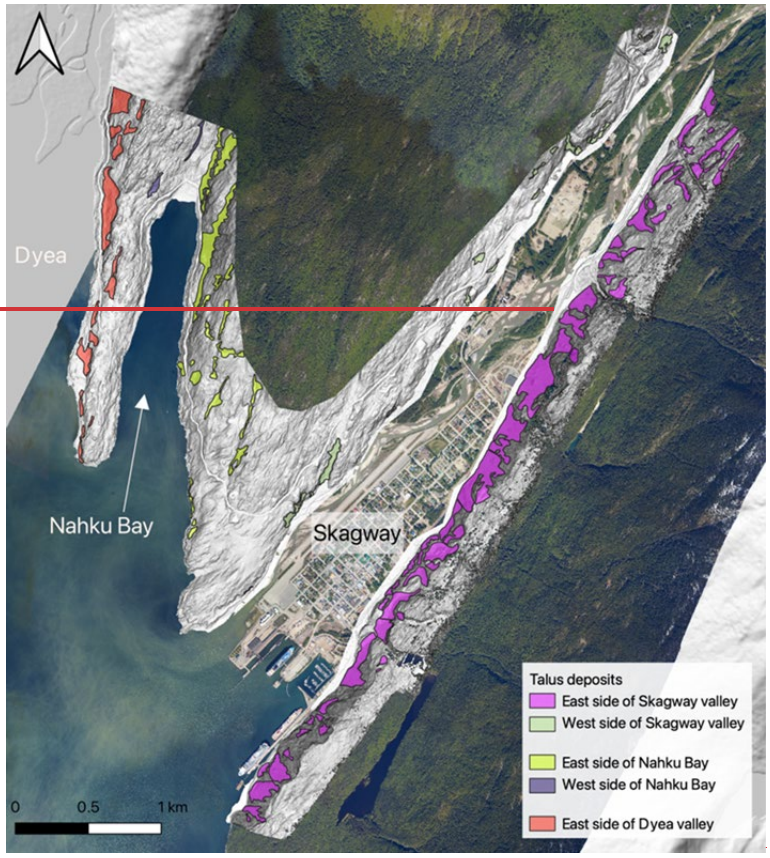

Figure 67: Distribution of talus deposits (yellow polygons), AKDOT&PF rockfall geoevents (2005-2022) (white/black dots), and Eastern ridge bedrock escarpment (red lines) ~~in study area~~. ~~Polygons identified by their location: Skagway River valley, Nahku Bay, and Dyea valley.~~ Note the abundance of talus deposits on the NW-facing ridgeline in Skagway and on NW-facing slopes in Nahku Bay and ~~near~~ along Dyea Road~~a~~. ~~Hillshade derived from DGGS lidar data.~~ Background image from USGS NAIP (National Agriculture Imagery Program). Merged lidar hillshade image has 50% transparency.

Formatted: Normal

Our lidar~~-~~ and field~~-derived~~ mapping revealed abundant talus slopes on northwest-facing ridgelines across our study area. ~~More~~ More generally, talus deposits compose 12% of the 7.2 km² total mapped area (Fig. 7). Along the eastern ridgeline, we identified abundant ~~56~~ talus slopes ~~with an average area of 9,290 m²,~~ which collectively make up 2~~5~~0% of that ridgeline area. On the west side of the ~~lower~~ Skagway River valley, the southeast-facing ridgeline hosts ~~20 talus deposits, and these talus slopes~~sparse talus cover that constitutes only 3% of ~~the 1.67 km² mapped area on~~ that side of the valley. Similarly, talus deposits on the southeast-facing ridgelines bordering Nahku Bay are much less abundant (1%) and smaller in area than on the northwest-facing ridgeline that abuts the bay (11%). In summary, talus slopes are significantly more abundant on NW-facing slopes across our study area and their location tends to correspond with AKDOT&PF geoevents along Dyea Road (Fig. 7).

4.3 Bedrock structure and discontinuities

To characterize the geometry of discontinuities with the potential to generate rockfalls, we collected ~~337~~ 405 joint orientations from 48~~36~~ granodiorite outcrops across the study area ~~(Supplemental material)~~ (Fig. 8a, supplemental materials) and plotted the data as poles to planes ~~on an equal area stereonet~~ on an equal area stereonet to identify dense clusters of poles which were then grouped into joint sets (Fig. ~~7~~8b-e). ~~Three~~ Two dominant joint sets were identified in this survey~~, two steeply dipping orthogonal sets~~ (*J1 & J2*), which are steeply dipping and approximately orthogonal (Fig. 8e)~~, and one set that dips gently to the west (J3)~~. The steeply dipping joints ~~are of relevance, as they tend to b~~are conducive to toppling, which is the most observed failure mode in Skagway. The most densely defined joint set is J1, which parallels the strike of the lower Skagway River valley and the eastern ridgeline and predominantly dips to the southeast. The less densely defined joint set (*J2*), is approximately orthogonal to *J1*, has near vertical dips, and strikes northwest.

We subsampled the joint orientation data in three geographic zones at the corners of our study area in order to assess the consistency of the rock structure. Joint orientations from the western portion of the study area are remarkably similar to those observed in the eastern and southern sections of our study area (Fig. 8b-d). This finding supports our use of the same bedrock structure data for kinematic analysis across the entire study area. ~~The third, gently dipping joint set (J3), are interpreted as sheeting joints, typical in plutonic rocks, which have significantly higher curvature at the outcrop scale than the steeply dipping orthogonal joints resulting in an elongate field of poles on the stereonet.~~

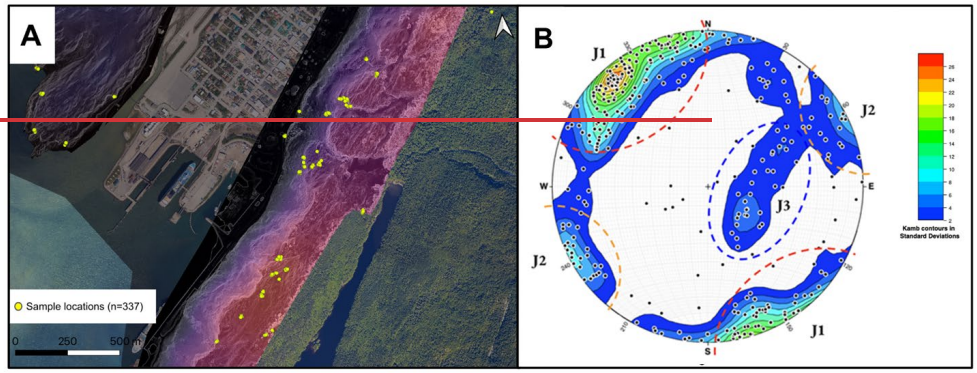

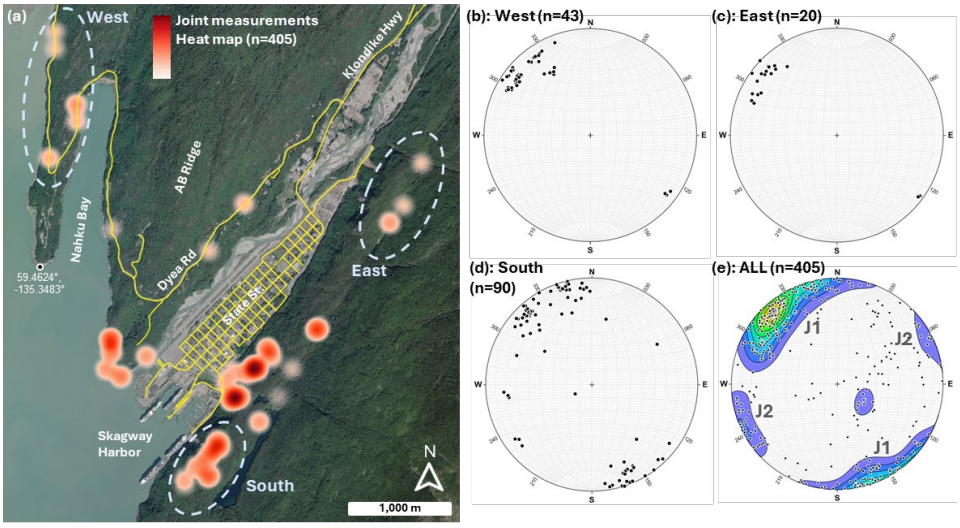

Figure 7~~8~~: ~~Structural~~ Joint survey data. (a) Location of ~~337~~ 405 structural measurements from ~~36~~ 48 outcrop locations ~~distributed across Skagway Valley and the AB ridgeline separating Skagway from Nahku Bay~~ with heat map showing relative abundance and dashed ellipses showing subsampled data shown in panels b-d. ~~See Fig. 4 for location.~~ (b-e) Lower hemisphere equal area stereonet plots of joint measurements visualized as poles to planes for West (b), East (c), South (d), and ALL joint data (e). The plot in e shows ~~(n=337) with~~ Kamb contours to highlight dense clusters of poles (warm colors reflect high density and cool colors convey low density) and~~, which were grouped into~~ three joint sets (J1, J2, and J3)two dominant joint sets (J1 and J2) are labeled. Background image in (a) from USGS NAIP (National Agriculture Imagery Program).

4.4 Kinematic analysis of rockfall susceptibility

Finally By combining equations 1 and 2 with our joint orientation data (Fig. 8) and merged lidar dataset (Fig. 4), we mapped susceptibility to planar sliding and block toppling, respectively, across our study area (Fig. 9a,b). , wTerrain susceptible toe observe small areas of terrain with planar failure is sparse and 83% of the terrain has zero values of susceptibility such that none of the measured joint orientations satisfy the planar sliding criteria. Furthermore, the terrain with non-zero planar sliding susceptibility values has very low values with a small fraction exceeding 5% (Fig. 9c)susceptibility according to equation 1 and in these patches, less than 5% of the joints are predicted to promote planar sliding. By contrast, our analysis demonstrates that 29% of the terrain has non-zero values of block toppling susceptibility and a substantial fraction of the non-zero values exceed 5% (Fig. 9d). This result emerges because tThe abundance of consistently oriented joints with vertical or sub-vertical dips suggests that rock promotes block toppling is the dominant rockfall mechanism in Skagway, which is supported by field observations. Furthermore, given the consistent orientation of sub-vertical joints across our study area (Fig. 8), the primary control on rockfall susceptibility to toppling is the orientation and inclination of rock faces according to equation 2(equation 2). On Along the crest of the eastern ridgeline inridge that borders the eastern lower Smargin of Skagway River valley, for example, the glacially flattened bench at the ridge crest top of the slope is not steep enough (<20°) to meet topographic conditions for either failure mode (Fig. 9a,b) (Fig. 5). As one movesMoving to the west side of the crest, however, the gentle ridgetop abruptly transitions to the steep escarpment where overhanging, cliffy bedrock slopes are perched above extensive talus deposits observed(Fig. 7). At this position on the ridgeline,In these locations, our analyses show that large patches of terrain have that a substantial portion (>-2055%) of discontinuities observed jointsthat promote toppling failure according to equation 2 (see deep red colours in Fig. 9b)8). At downslope locations (i.e., between the ridgeline and valley floor)Furthermore downslope, we observerock slopes continue to exhibit patchy zones of high toppling susceptibility, many of which are in close proximity to Skagway township and harbour. Along the southeast-facing rock slopes on that border the west side side of Skagway, our analyses reveal show fewer and smaller patches of terrain with toppling terrain susceptibility ble to toppling withapproximating less than 5-10%, indicating low susceptibility of the discontinuities predicted to be unstable. This asymmetric susceptibility pattern continues. We observe a similar pattern along the sub-parallel ridges west of Skagway along Dyea Road with west- and northwest-facing ridgelines exhibiting abundant patches of terrain with high propensity for toppling failure (Fig. 8)and east- and southeast-facing slopes showing negligible toppling susceptibility (Fig. 9b). Finally, we observe small areas of terrain with planar failure susceptibility according to equation 1 and in these patches, less than 5% of the joints are predicted to promote planar sliding. More generally, by combining our talus slope deposit maps with our toppling failure susceptibility maple zones, we note a strong correspondence such that zones with >5% toppling failure commonly tend to occur just upslope of talus-mantled slopes (Fig. 9b9). Furthermore, our maps show that zones with values of toppling susceptibility less than 5% tend to be more isolated and

less clearly connected with talus deposits. As a result, the 5% toppling susceptibility index value serves as an effective threshold for defining rockfall source areas.

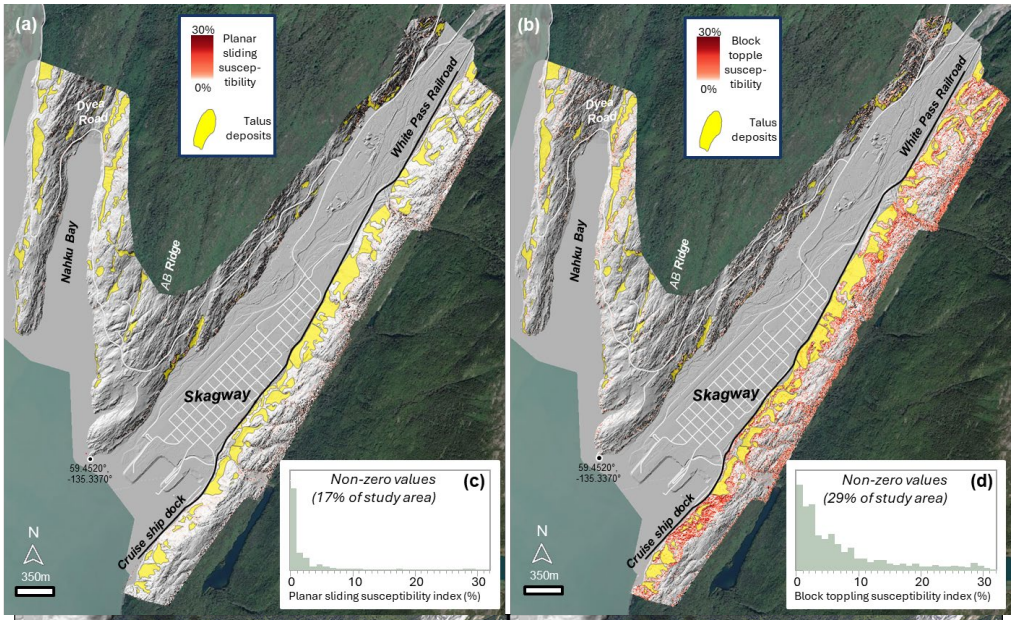
(a)
30%
Planar sliding suscep-tibility
0%
Talus deposits
Dyea Road
White Pass Railroad
Nahku Bay
AB Ridge
Skagway
59.4520°
-135.3370°
Cruise ship dock
N
350m
Non-zero values
(17% of study area)
(c)
0
10
20
30
Planar sliding susceptibility index (%)
(b)
30%
Block topple suscep-tibility
0%
Talus deposits
Dyea Road
White Pass Railroad
Nahku Bay
AB Ridge
Skagway
59.4520°
-135.3370°
Cruise ship dock
N
350m
Non-zero values
(29% of study area)
(d)
0
10
20
30
Block toppling susceptibility index (%)

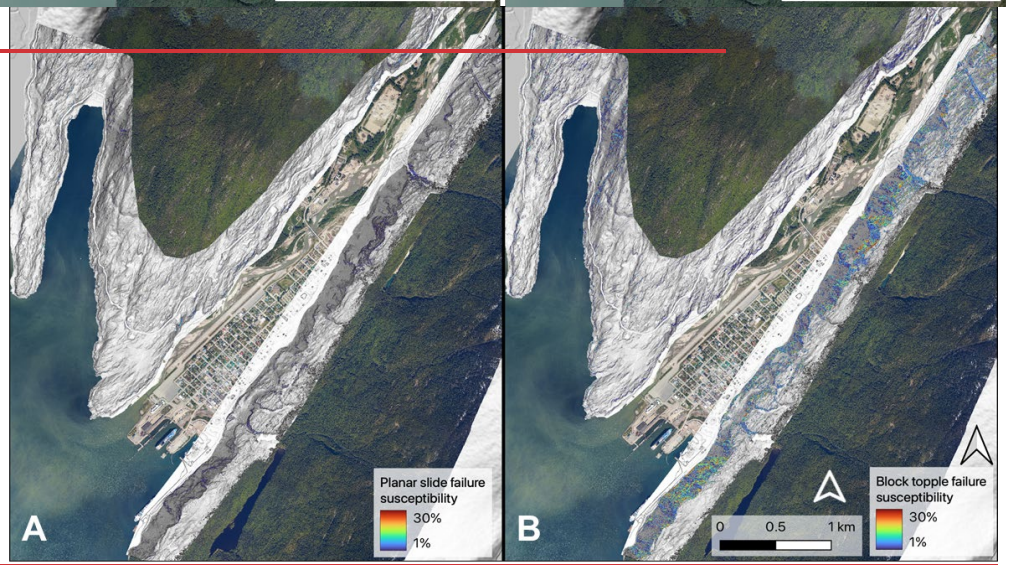
A
Planar slide failure susceptibility
30%
1%
B
0
0.5
1 km
Block topple failure susceptibility
30%
1%

600

Figure ~~8~~9: Maps of (a) ~~rockfall~~ planar sliding and (b) block toppling susceptibility ~~indices~~ indices using combined 2014 airborne and 2023 UAS lidar datasets and joint orientation data. Histograms of (c) planar sliding and (d) block toppling susceptibility indices for non-zero values. ~~. (a) Susceptibility to planar slide failure according to equation 1, and (b) susceptibility to block toppling according to equation 2. Both indices~~The mapped and plotted values are ~~are estimated as~~ the percentage of field-surveyed joints deemed unstable at each pixel according to equations 1 (planar sliding) and 2 (block toppling). Yellow polygons denote talus deposits. Note the abundance of toppling failure zones on NW-facing rock slopes that border Skagway and Nahku Bay as well as the correspondence between toppling susceptibility and talus deposits. Hillshade imagerys ~~in a and b~~ derived from ~~DGGS~~ combined 2014 and 2023 lidar data. Background image from USGS NAIP (National Agriculture Imagery Program).

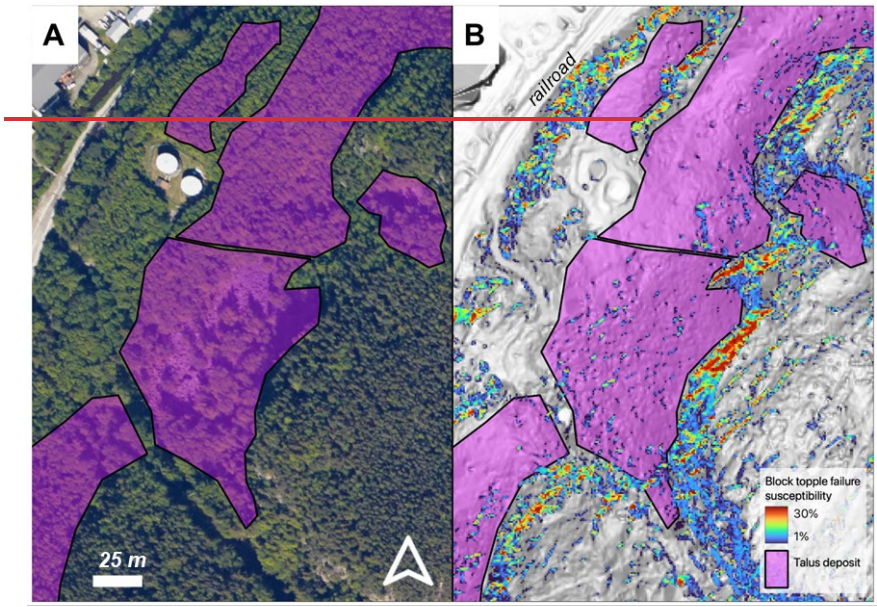

~~Figure 9: Map of talus deposits and block toppling susceptibility index (percentage of joints deemed unstable in each pixel according to equation 2). See Fig. 4 for location. (a) Orthoimage of Kirmse's cliff and the partially forested talus deposit at the base of the slope, (b) Block toppling susceptibility index. Note the abundance of susceptible toppling areas perched above the~~

Formatted: Normal

~~talus deposits. Background image in (a) from USGS NAIP (National Agriculture Imagery Program). Hillshade in (b) derived from DGGS lidar data.~~

4.5 Rockfall runout modelling using RAMMS

Using~~By using~~ zones of high toppling susceptibility (>5%) as source areas for rockfall initiation, we ~~used~~ applied RAMMS to model the runout of ~~nearly~~ 49,450~~50,000~~ rockfall events for each of the four scenarios that account for differences in ~~clast~~ block size and ground cover. We applied the runout model along the ridge bordering the eastern margin of Skagway and used the 5.4-km long section of the White Pass Railroad extended along the cruise ship dock to demarcate rockfall passages with potential impact to the harbour and township (Fig. 10a-e). The ridge is steeper in the southern (4500 to 5500 m on the railroad transect) and central (1500 to 3000 on the transect) sections where extensive bedrock cliffs protrude above talus deposits (Fig 10a). These cliffs are identified as zones of high toppling susceptibility and thus designated as rockfall source areas (Fig. 10b~~Our~~). Our simulations showing the ~~total~~ number of rockfall events ~~traversing~~ that pass through each pixel reveal distinct zones subject to high rockfall susceptibility as well as extensive downslope transport (Fig. 10c,d). For both the 50th block/dense forest and 95th block/fine talus scenarios shown here~~In each of the four scenarios~~, the southern end of the ridgeline above the harbour (between ~~4 and 5km~~4500 and 5500 on ~~our railroad-based~~ the transect) exhibits ~~~10~~>10 specific chutes or paths of ~~likely~~ efficient rockfall runout whereby initiation near the escarpment results in the concentration of rockfall runout along these paths and conveyance to the cruise ship docks and/or harbour ~~(Fig. 10)~~. Both scenarios exhibit a zone of events that pass across the railroad as depicted by the heat map (Fig 10c,d).~~This zone coincides with the area of high-relief terrain and extensive escarpment development.~~ In contrast, the central portion of the ridgeline (~~between 2.8 and 4km~~between 3000 and 4500m on the transect)~~)~~ immediately adjacent to much of the township exhibits patchy and less frequent rockfall activity along gentle and irregularly oriented bedrock steps and benches. Further north, our simulations ~~again~~ reveal abundant long rockfall runout paths at the northern extent of the township with ~~a concentration~~concentrated activity near the Cemetery Slide area (between 1~~ and 2km~~500 and 3000m on the transect) with a high concentration of blocks predicted to pass across the railroad (Fig 10d). Finally, at the northernmost extent of our simulation domain (from ~~near 1km~~0 to 1500m on the transect), the results show patchy and short rockfall transport paths coincident with gentle, benchy topography. Taken together, these simulations demonstrate a large fraction of the ridge has similar morphology and modelled rockfall runout behaviour as the zone of recent activity above the cruise ship dock. ~~Although the relative pattern of predicted runout described here is consistent across the four scenarios, our simulations of 95th percentile size clasts and no forest cover result in the most abundant passage of rockfall events to the valley floor with high potential for impacting infrastructure and imperilling public safety (Fig. 10d).~~

Formatted: Superscript

Formatted: Superscript

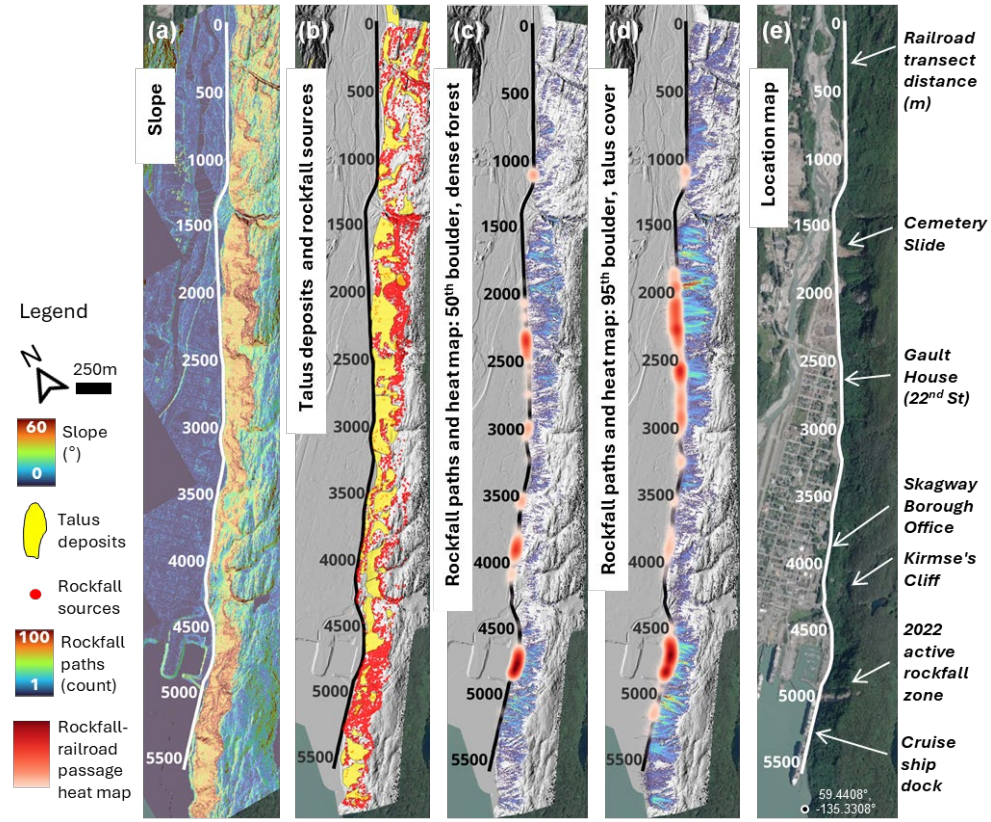
(a)
(b)
(c)
(d)
(e)
Slope
Talus deposits and rockfall sources
Rockfall paths and heat map: 50th boulder, dense forest
Rockfall paths and heat map: 95th boulder, talus cover
Location map
Railroad transect distance (m)
Cemetery Slide
Gault House (22nd St)
Skagway Borough Office
Kirmse's Cliff
2022 active rockfall zone
Cruise ship dock
59.4408°, -135.3308°
Legend
250m
Slope (°)
Talus deposits
Rockfall sources
Rockfall paths (count)
Rockfall-railroad passage heat map

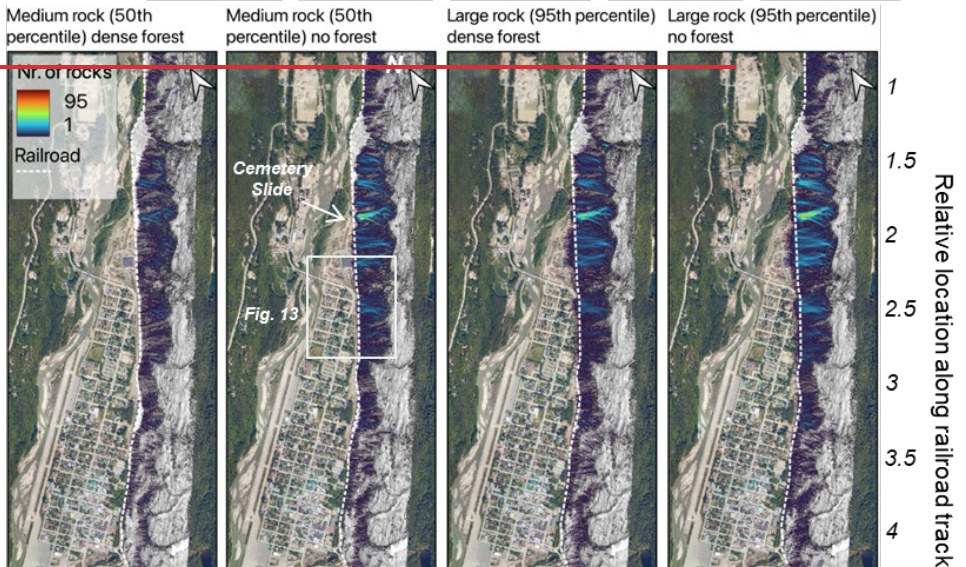
Medium rock (50th percentile) dense forest
Medium rock (50th percentile) no forest
Large rock (95th percentile) dense forest
Large rock (95th percentile) no forest
Nr. of rocks
95
1
Railroad
Cemetery Slide
Fig. 13
Relative location along railroad track

Figure 10: Map of topography and rockfall models along the ridgeline that abuts Skagway township and Harbor. (a) Map of slope angle using merged 2014 airborne and 2023 UAS lidar, (b) Map of rockfall sources (red points) and talus deposits (yellow polygons), (c, d) Maps of modeled rockfall ~~runout~~ paths ~~along eastern ridgeline in Skagway Valley conducted~~ for ~~4~~ 2 scenarios with variable ~~clast~~ block size and land cover. ~~(panels a-d).~~ The number of rockfall events that traverse each ~~cell~~ pixel is indicated by the color ramp ~~with warm colors reflecting frequent rockfall passage~~. Heat map (red shades) denotes relative density of modeled rockfalls that pass over the railroad, ~~Note the abundance of long runout events in the SW section bordering the harbour and near the northern extent of the township. The dashed white line denotes the railroad track used to document rockfall runout and kinetic energy in Fig. 11 for relative position along the tracks. The white box in (c) denotes the area shown in Fig. 13, site of an historic rockfall event that impacted the township.~~ (e) Satellite image from USGS NAIP (National Agriculture Imagery Program) with annotated locations indicated. All maps include railroad transect demarcations. Hillshade images in (b-d) derived from ~~DGGS~~ merged lidar datasets. ~~lidar data. Background image from USGS NAIP (National Agriculture Imagery Program).~~

To ~~characterize the location and potential impact of simulated rockfall events that reach the valley floor~~assess controls on rockfall propagation susceptibility along the railroad transect, we tallied the number ~~and kinetic energy~~ ~~o~~of simulated rockfall events that traverse the railroad track and quantified topographic properties of the ridge (Fig. 11). Although the railroad-to-ridge distance (or ridge width) is relatively consistent along the transect, the density of rockfall source areas varies substantially (Fig. 11a). The southern section of the ridge (4500 to 5400m) has a concentration of toppling source areas, which is ~4x higher than slopes in the central section (2500 to 4000m) of our transect. Another zone of high source density occurs at ~2000m on the transect and values to the northern extent are low to moderate in magnitude. Average slope angle along the ridge varies substantially with high values (>35°) in the southern (4500 to 5400m) and north-central (1500 to 2500m) sections and low values in the south-central section (3000 to 4500m) (Fig. 11b). Average values of slope roughness (estimated as the standard deviation of slope estimated for local windows with 5m radius) are relatively high in the southern section of the transect and low in the central section before increasing monotonically to the north (Fig. 11b). Notably, our analysis shows that slope angle, rockfall source density, and roughness exhibit distinctive patterns along the ridge enabling us to distinguish their influence on the modelled runout pattern.

Although the relative pattern of simulated runout is consistent for the two scenarios shown here (Fig. 10c,d), our transect analysis shows that only 1.2% of the simulated events for the 50th block/dense forest scenario result in passage across the railroad whereas 19.1% of the 95th block/fine talus scenario events travel across the railroad (Fig. 11c,d). In several sections, the passage fraction for the 95th block/fine talus scenario exceeds 50%, implying that the destabilization of a large block will likely result in downslope impacts (Fig 11d). By contrast, the passage fractions for the 50th block/dense forest scenario rarely exceed 4% such that unstable blocks have a low probability of impacting the valley (Fig 11c). This disparity reveals the profound influence of block size and land cover on rockfall propagation susceptibility. Furthermore, the modelled runout patterns reveal how slope morphology controls rockfall propagation. In both scenarios, sections of the ridge with high passage fractions correspond with low roughness values and the zone of high roughness at 4000 to 4500m on the transect

Formatted: Superscript

Formatted: Superscript

Formatted: Superscript

corresponds with negligible rockfall passage (Fig 11b). ~~In each of these scenarios, the north-to-south alternating pattern of high-low rockfall runout hazard is reflected in the number and kinetic energy of clasts that travel to the base of the ridgeline. Given the 49,450 simulated rockfall events in each of the four scenarios, <2% and 12% rocks crossed the railroad for the dense forest and no forest scenarios with the 50th percentile clast size, respectively. By contrast, using the 95th percentile clast size resulted in nearly 20% and 28% rockfall passage of the railroad in the dense forest and no forest scenarios, respectively. These results highlight the importance of dense forest and clast size in determining risk of rockfall runout.~~ By contrast, our analyses show that mean slope angle and rockfall source density do not strongly correlate with the pattern of rockfall passage across the railroad.

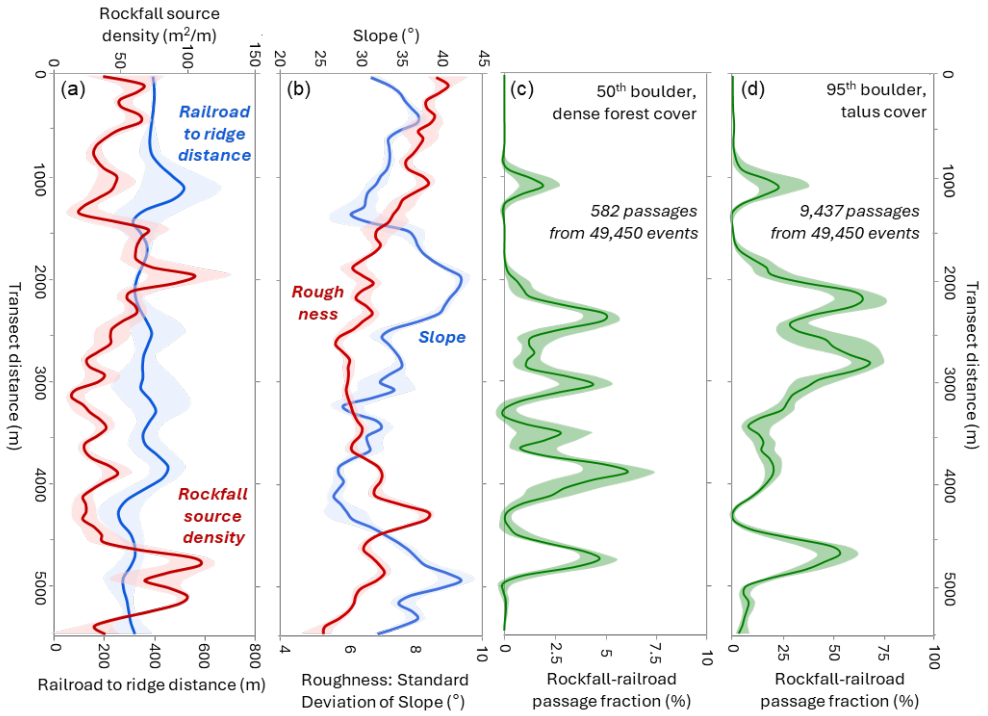
Rockfall source density (m²/m)
Slope (°)
(a)
(b)
(c)
(d)
Railroad to ridge distance
Rockfall source density
Rough ness
Slope
50th boulder, dense forest cover
582 passages from 49,450 events
95th boulder, talus cover
9,437 passages from 49,450 events
Transect distance (m)
Railroad to ridge distance (m)
Roughness: Standard Deviation of Slope (°)
Rockfall-railroad passage fraction (%)
Rockfall-railroad passage fraction (%)

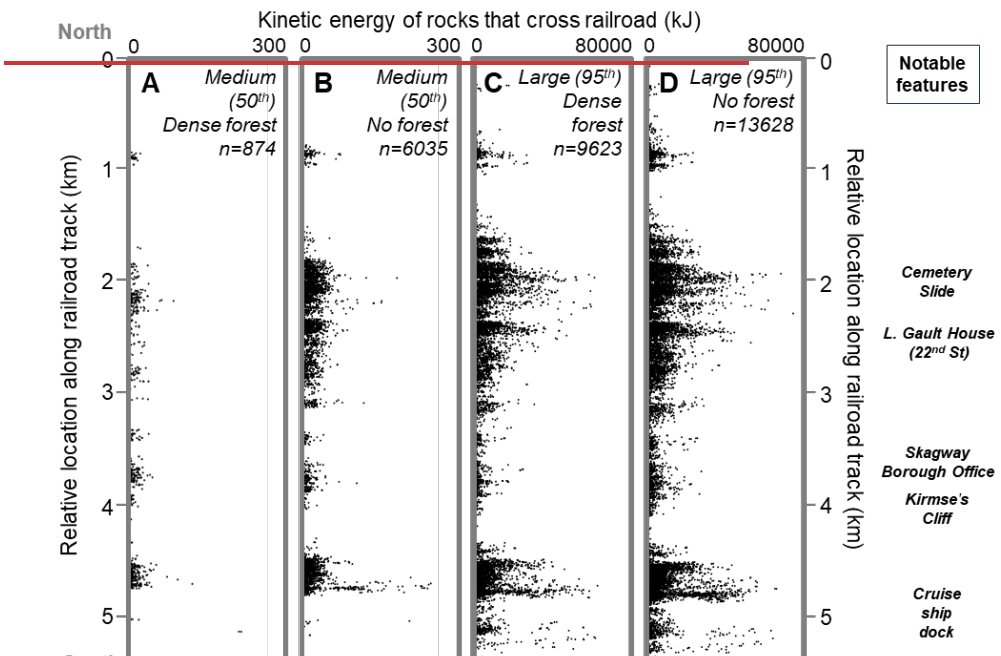
Kinetic energy of rocks that cross railroad (kJ)
North
A Medium (50th) Dense forest n=874
B Medium (50th) No forest n=6035
C Large (95th) Dense forest n=9623
D Large (95th) No forest n=13628
Relative location along railroad track (km)
Notable features
Cemetery Slide
L. Gault House (22nd St)
Skagway Borough Office
Kirmse's Cliff
Cruise ship dock

Figure 11: Plots of rockfall model variables and topographic properties along the railroad transect that bisects Skagway and the rockfall prone ridgeline (see Figure 10 for location). (a) Profile of rockfall source density (m^2 m^{-1}), which depicts the upslope area of toppling-prone terrain (normalized by distance along transect) calculated with equation 2 for terrain between the railroad and the ridge crest, and plot of the horizontal distance between the railroad and ridge crest, (b) Profile of average slope and roughness (estimated as standard deviation of local slope within a 5-m radius window) for terrain between railroad and the ridge crest, (c) Profile of modeled rockfall-railroad passage percentage for the scenario with 50th percentile block size and dense forest cover, and (d) Profile of modeled rockfall-railroad passage percentage for the scenario with 95th percentile block size and fine talus land cover. Shaded intervals convey standard deviation of values in all plots.

Formatted: Superscript

Formatted: Superscript

~~Kinetic energy of simulated rocks that pass the railroad tracks (see Fig. 10 for location) for 4 scenarios with variable clast size and land cover (panels a-d). Note the difference in scale of kinetic energy between panels (a,b) and (c,d). The number of rocks that pass across the track is highest for the scenario with the largest clast size and no forest cover. Notable locations are annotated along the right margin of the plots.~~

5 Discussion

Although r~~R~~ainfall has been~~appears to be~~ responsible for triggering some notable rockfall events in Skagway, ~~but a~~ substantial seasonal increase in~~the majority of~~ rockfall events documented in the AKDOT&PF inventory occurred in late March and April. This period corresponds to rapid increases in temperatures, particularly the minimum daily temperature, which implies that thawing of ice, snow, and rock mass may contribute to increased activity (Fig. 6).~~are not preceded by heavy precipitation.~~ This observation is consistent with many studies that have documented thermal-driven rockfall activity in alpine environments in Europe and elsewhere~~(Draebing et al., 2022; Gruber et al., 2004; Krautblatter et al., 2013; Matsuoka and Sakai, 1999)~~; the proposed mechanisms include active layer thaw, ice-filled fracture destabilization, and thermal stress cycles, with peak activity typically occurring during spring and early summer months when temperatures rise above freezing (Draebing et al., 2022; Gruber et al., 2004; Krautblatter et al., 2013; Matsuoka and Sakai, 1999; Mayer et al., 2024). Given that the low-elevation rock slopes around Skagway are too warm to support permafrost, ice-filled fracture destabilization may be a relevant mechanism. Field-based studies have noted cleft ice in rockfall scars which implies that ice segregation processes during cold periods followed by warming and thaw-induced weakening can destabilize fractured rock masses (Huggel et al., 2012; Ravanel et al., 2013). Dendrochronological studies in Switzerland reveal that 88% of rockfall scars occur between mid-October and end of May, with peak activity in April when ice lenses formed from meltwater slowly infiltrate into fractures (Stoffel et al., 2005). These studies highlight the critical role of spring thaw in destabilizing previously frozen rock masses which may be relevant to the timing of rockfall activity in Skagway. Nonetheless, the specific timing of seasonal activity remains challenging to predict, motivating efforts to determine the spatial pattern of rockfall initiation and propagation susceptibility to mitigate hazard.

~~Therefore, accurately predicting the timing of rockfall events based on precipitation metrics, like rainfall initiation thresholds used to estimate the likelihood of landslide initiation in Sitka, AK (Patton et al., 2023), is not likely to be successful. Instead, estimating the spatial pattern of rockfall susceptibility is a useful approach to mitigating rockfall hazard.~~ Taken together, our analyses of ~~rockfall~~ block toppling susceptibility and talus deposition maps demonstrate that rockfall source areas and runout paths tend to be ~~located~~ situated on northwest-facing rock slopes in the ~~lower~~ Skagway River valley, Nahku Bay, and ~~the~~ lower Taiya River valley. Our joint dataset~~,~~ suggests that this ~~indicating a~~ strong topographic control on rockfall activity ~~owing~~ owes to the coincident ~~regularity~~ alignment of glacial valleys and joint orientation~~s in the area.~~s, both of which are remarkably consistent in the area.

The joints measured in this study are consistent with the steeply dipping, orthogonal joint sets measured in a nearby (~15km northwest of Skagway) structural survey in ~~West Creek~~on a tributary to the Taiya River (Callahan and Wayland, 1965) and described in a geotechnical assessment of the rock slopes above Skagway's cruise ship dock (Brennan and Whistler, 2022). These h~~H~~igh angle joints are likely formed by the tensile component of shearing from the nearby Chatham Strait fault and Eastern Denali fault systems~~, while sheeting joints reflect the combined influence of far field tectonic stresses and topographic stress that arise from landscape curvature (Martel, 2006, 2017)~~. Rock slopes with orthogonal jointing are often predisposed to block toppling failure particularly where steep orthogonal joints form the sides of toppling blocks and low angle joint~~s, like the sheeting joints observed in this study,~~ s act as the basal failure plane (Wyllie and Mah, 2004). ~~Because the densest cluster of joints we observed dips steeply to the southeast, rock slopes facing northwest tend to form anti-dip slopes which are conducive to toppling failure. This is supported by larger and more abundant talus deposits on the east sides of the lower Skagway River valley and Nahku bay, confirming that rockfall occurs preferentially on northwest-facing slopes (Fig. 6).~~

The results of our kinematic analysis demonstrate that rock slopes in the steep rugged terrain surrounding Skagway are ~~more~~ highly susceptible to block toppling failure~~failure than planar slide failure~~. The preference for topping failure is due to the steep inclination of joints, which are ~~generally steep and~~ conducive to toppling failure as their near verticality ~~may~~ tends to preclude ~~them~~ them from daylighting in rock slope faces, a necessary condition for planar slid~~e~~ing or wedge~~e~~ failure (Figure 1). The abundance of talus deposits situated just downslope of zones with high toppling susceptibility (Fig. 9b) is consistent with other studies (Guerriero et al., 2024) and supports the utility of our modelling approach. More advanced treatments that explicitly account for individual trees, land cover features, and source block geometry would improve the local accuracy of our simulations although the regional-scale results presented here are robust and helpful for informing mitigation efforts. ~~On the west side of the lower Skagway River valley, an isolated zone of steep vertical cliffs is susceptible to planar slide failure~~

~~as recent planar failures are evident, which release from sheeting joints and slide on joints steeply dipping southeast (Fig. 12).~~

Consistent with previous studies (e.g., Loye et al., 2009), our r

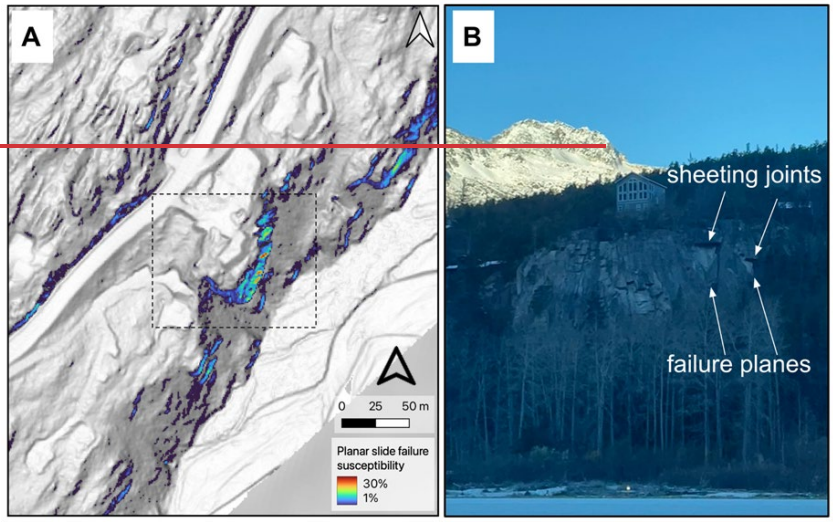

~~Figure 12: Planar sliding susceptibility along the western ridgeline in Skagway River Valley. Location depicted in Fig. 4. (a) Map of planar failure susceptibility index using equation 1. (b) Image of SE-facing ridgeline in lower Skagway River valley. Note high values on SE-facing steep bedrock cliffs that coincide with field evidence for sheeting joints and planar failures. Hillshades derived from DGGS lidar data.~~

~~R~~ockfall susceptibility maps are consistent with the failure mode and location of rock slope deformation observed in the field. ~~Just~~On the uphill side of the prominent escarpment along the eastern ridgeline in the lower Skagway River valley (Fig. 7), we observed numerous instances of detached parallel slabs of rock separated by open tension cracks that extend downward for several meters (Fig. 3). These blocks appear to be experiencing the early phases of toppling failure as vegetation and other environmental perturbations ~~processes~~ can contribute to crack widening (Pawlik et al., 2016; Rempel et al., 2016). These observations also indicate that our predicted zones of toppling failure ~~along active bedrock escarpments~~ are likely to continue propagating southeast with the active bedrock escarpment ~~to the southeast~~ providing additional blocks ~~available~~ to initiate rockfall. More generally, these observations suggest that erosion and ~~SE~~southeast-oriented lateral

migration of the ~~eastern~~ ridgeline has been substantial since ~~the~~ glacial retreat 10 to 12 kya. Approximate r~~R~~econstruction of the ridge~~line (Moore et al., 2009)~~ to its immediate post-glacial geometry (Moore et al., 2009) implies that 10 to 100 meters of lateral erosion has occurred during the Holocene. The linear character of the escarpment and pervasive indicators of active toppling also imply parallel retreat over geomorphic timescales, which occurs given the favourable combination of dip and slope angle as well as erosion rate (Imaizumi et al., 2015). As such, ~~On-going rockfall activity along this ridgeline suggests that this~~the unravelling and lateral retreat ~~of the~~of the escarpment will likely continue until the interface encounters a different configuration of slope and structural geometry. ~~continue.~~

~~Importantly~~As our simulations demonstrate, extensive rockfall activity and lateral divide migration does not occur along the entire ridge~~line~~. Rather, our results show large sections ~~of the 5 km long ridgeline~~ with patchy and localized talus deposits and benchy bedrock landforms that arises because of variations in the depth and pattern of glacial erosion. On Kirmse's Cliff (at 4200m~~4 km~~ on the ~~railroad~~ transect, Fig. 10e), for example, talus deposits extend upslope from the valley floor to vertical cliff faces that terminate at the ridgeline (Fig. 5). In this area, ~~rockfall~~ toppling susceptibility is relatively high, but concentrated in a relatively small area of vertical rock slope, and a forested talus deposit and benchy zone sits between the cliff and ~~infrastructure in Skagway~~the valley floor (Fig. 10b~~9~~). By contrast, several areas along the escarpment exhibit high potential for rockfall runout to reach the valley. At the cruise ship dock (4500m on the transect~~.5 to 5 km~~), continuous, rockfall-prone slopes above the cruise ship dock span from the escarpment to the base of the slope, resulting in a large area with high rockfall propagation susceptibility in close proximity to harbour infrastructure. Similarly, from ~~1.5 to 2.5 km~~1500 to 2000m on our railroad transect, a high-relief escarpment with steep vertical bedrock outcrops near the crest exhibits a continuous steep slope to the valley floor (Fig. 10a). In this area, which is the source area for the Cemetery Slide, rockfall susceptibility and long runout potential are high and we observed frequent spalling and rolling rocks traversing the talus deposits during our field work (Fig. 10c,d~~b~~). ~~In additio~~In fact~~n~~, The Daily Alaskan reported a 1914 rockfall event just south of the Cemetery Slide at ~~2.5km~~2500m along the transect which coincides with our simulations of high rockfall runout potential (Figs. 10c,d~~0 & 13~~). During that event, L. Gault noted “an avalanche of earth and stone” that “leaped the railroad track…pounding against the fence.” Gault also noted that the railroad track served as a “safety barrier” because “the force of the descent had been so much lessened.” Further afield in the ~~NE~~ northeast section of Nahku Bay, another zone of high rockfall susceptibility is revealed by our analysis. Steep rocky slopes rise to an elevation of 250 m with close proximity to Dyea Road (Fig. 7). This area lacks a well-developed runout path, but it does coincide with source areas for ~~two~~ dozens of events in the AKDOT rockfall inventory that impacted Dyea Road. ~~Most generally, a rigorous characterization of rockfall risk in Skagway requires estimation of occupation and usage of structures and transportation corridors coupled with our results (e.g., Michoud et al., 2012).~~

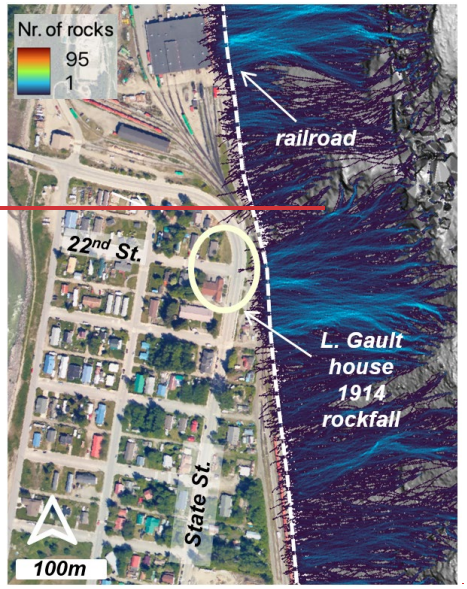

~~Figure 13: Detailed map of modeled rockfall runout (Medium rock (50th percentile), no forest) with location depicted shown by white box on Fig. 10b. Note the location of rockfall near the intersection of 22nd and State Street described by L. Gault in the March 26, 1914, edition of The Daily Alaskan. That location corresponds with a region of likely rockfall runout identified by our coupled initiation-runout simulations. Hillshade derived from DGGS lidar data. Background image from USGS NAIP (National Agriculture Imagery Program).~~

Our analyses reveal distinctive zones of high rockfall initiation and runout (or propagation) susceptibility ~~hazard~~ in the Skagway region that result from the combination of glacial erosion that sets the morphology of bedrock slopes and the orientation of joint sets that determine the geometry of potential bedrock failures. Most likely, the orientation and extent of glacial erosion is not independent of the joints (Hooyer et al., 2012; Krabbendam and Glasser, 2011). Rather, we suspect that the nearly parallel orientation of joints and the N-NE trending ridge~~line~~ along the eastern margin of the ~~lower~~ Skagway River valley arise due to glacial erosion tracking discontinuities that facilitate erosion more readily than undeformed bedrock. ~~Localized zones of the prominent ridgeline that abuts Skagway River valley exhibit abundant historic rockfall activity and over long timescales this activity is likely to continue. As such,~~ This long-term evolution implies feedbacks between rock structure and bedrock erosion processes from glaciers and rockfalls that support strong gradients in rockfall activity. ~~o~~ In assessing how these factors moderate the current hazard context, our findings critically depend on the combination of

kinematic modelling and runout susceptibility to provide ~~key~~ constraints for identifying areas at risk to inform mitigation efforts. ~~Most generally~~Additional work is needed, however, to conduct~~,~~ a rigorous characterization of rockfall risk in Skagway ~~requires~~that includes estimation of occupation and usage of structures and transportation corridors to be coupled with our results (e.g., Michoud et al., 2012).

6 Conclusions

The integrated kinematic analysis and the runout modelling presented here matches well with field observations and provides the basis for a sophisticated approach in rockfall hazard assessment. ~~Rock slope failure is a major driver of landscape evolution in Skagway since glacial retreat.~~ The steeply dipping orthogonal joints in Skagway's rock slopes are highly conducive to block toppling failure which has resulted in highly asymmetric rockfall susceptibility. Our results highlight a distinct contrast in the morphology of Skagway River valley's eastern and western ridgelines, which is primarily determined by the predisposition of northwest-facing slopes to block toppling failure along a densely fractured joint set that dips steeply to the southeast. This is consistent with geomorphic evidence of extensive rockfall activity, where talus deposits are more abundant and larger on the eastern side of the lower Skagway River valley than the west. This structural control on rockfall activity is also ~~reflected~~ evident in the east and west sides of Nahku Bay, situated to the west of Skagway. ~~Historic rockfall records~~Our analysis of a rockfall inventory indicates a similar preference for initiating on northwest-facing slopes and reveal a seasonal peak in rockfall activity in late March and April that likely results from thawing of ice-filled joints and reduction of rock mass strength. Our simulations of rockfall runout show areas with high rockfall susceptibility that may merit further investigation and mitigation: 1) the ridgeline and slopes above the cruise ship dock, 2) the high-relief topography at the north end of Skagway ~~(which includes the Cemetery Slide)~~, and 3) the eastern ridgeline bordering Nahku Bay. Recent rockfall source areas located in these regions are characterized by steep northwest~~-~~facing slopes that are highly susceptible to block toppling failure and reach >200 m in elevation which facilitates long runout paths. Our results also demonstrate that slope roughness over ~10m scales serves as a better predictor of rockfall propagation that slope angle and the density of rockfall source areas. Our integrated modelling approach and field assessment provides a simple but robust approach to assess rockfall hazard.

7 Data availability

All topographic data used for analyses are cited within the text. The structural data are available as Supplemental material.

8 Author contribution

IW and JR conceived and designed the study and IW and JR~~W~~ executed the study, RC provided on-site context, knowledge and guidance, AP contributed to study design and fieldwork, IW and JR prepared the manuscript with contributions from all other co-authors.

9 Acknowledgments

This research was funded by NSF Award #2052972 (Focused CoPe: Building Community Sensor Networks for Coastal Hazards and Climate Change Impacts in Southeast Alaska), which supports community-driven fundamental and translational geohazard science for project partners across SE Alaska. The authors thank leaders and members of the Skagway Traditional Council and residents of Skagway for their observations, critical insights, hospitality, and field assistance; the Municipality of Skagway for sharing rockfall reports; and the NSF-funded UW RAPID facility for the timely acquisition of UAS lidar data. Conversations with Joe Wartman, Ben Leshchinsky, alex grant, Chris Massey, and Dimitrios Zekkos were insightful and contributed to our understanding of ~~rockslope~~rock slope processes.

10 References

Abellán, A., Calvet, J., Vilaplana, J. M., and Blanchard, J.: Detection and spatial prediction of rockfalls by means of terrestrial laser scanner monitoring, Geomorphology, 119, 162–171, https://doi.org/10.1016/j.geomorph.2010.03.016, 2010.

Abellán, A., Vilaplana, J. M., Calvet, J., García-Sellés, D., and Asensio, E.: Rockfall monitoring by Terrestrial Laser Scanning – case study of the basaltic rock face at Castellfollit de la Roca (Catalonia, Spain), Natural Hazards and Earth System Sciences, 11, 829–841, https://doi.org/10.5194/nhess-11-829-2011, 2011.

Aksoy, H. and Ercanoglu, M.: Determination of the rockfall source in an urban settlement area by using a rule-based fuzzy evaluation, Natural Hazards and Earth System Sciences, 6, 941–954, https://doi.org/10.5194/nhess-6-941-2006, 2006.

Alejano, L. R., Veiga, M., Pérez-Rey, I., Castro-Filgueira, U., Arzúa, J., and Castro-Caicedo, Á. J.: Analysis of a complex slope failure in a granodiorite quarry bench, Bull Eng Geol Environ, 78, 1209–1224, https://doi.org/10.1007/s10064-017-1160-y, 2019.

Allen, S. and Huggel, C.: Extremely warm temperatures as a potential cause of recent high mountain rockfall, Global and Planetary Change, 107, 59–69, https://doi.org/10.1016/j.gloplacha.2013.04.007, 2013.

Baichtal, J. F., Lesnek, A. J., Carlson, R. J., Schmuck, N. S., Smith, J. L., Landwehr, D. J., and Briner, J. P.: Late Pleistocene and early Holocene sea-level history and glacial retreat interpreted from shell-bearing marine deposits of southeastern Alaska, USA, Geosphere, 17, 1590–1615, https://doi.org/10.1130/GES02359.1, 2021.

Bajni, G., Camera, C. A. S., and Apuani, T.: Deciphering meteorological influencing factors for Alpine rockfalls: a case study in Aosta Valley, Landslides, 18, 3279–3298, https://doi.org/10.1007/s10346-021-01697-3, 2021.

884 Ballantyne, C. K.: A general model of paraglacial landscape response, The Holocene, 12, 371–376,
885 https://doi.org/10.1191/0959683602hl553fa, 2002.

886 Barlow, J., Lim, M., Rosser, N., Petley, D., Brain, M., Norman, E., and Geer, M.: Modeling cliff erosion using negative power
887 law scaling of rockfalls, Geomorphology, 139–140, 416–424, https://doi.org/10.1016/j.geomorph.2011.11.006, 2012.

888 Biegel, K. M., Gosselin, J. M., Dettmer, J., Colpron, M., Enkelmann, E., and Caine, J. S.: Earthquake Relocations Delineate a
889 Discrete Fault Network and Deformation Corridor Throughout Southeast Alaska and Southwest Yukon, Tectonics, 43,
890 e2023TC008140, https://doi.org/10.1029/2023TC008140, 2024.

891 Bodin, X., Schoeneich, P., Deline, P., Ravanel, L., Magnin, F., Krysiecki, J.-M., and Echelard, T.: Mountain permafrost and
892 associated geomorphological processes: recent changes in the French Alps, Journal of Alpine Research | Revue de géographie
893 alpine, https://doi.org/10.4000/rga.2885, 2015.

894 Booth, A. M., LaHusen, S. R., Duvall, A. R., and Montgomery, D. R.: Holocene history of deep-seated landsliding in the North
895 Fork Stillaguamish River valley from surface roughness analysis, radiocarbon dating, and numerical landscape evolution
896 modeling: Landsliding in the N. Fork Stillaguamish, Journal of Geophysical Research: Earth Surface, 122, 456–472,
897 https://doi.org/10.1002/2016JF003934, 2017.

898 Borella, J., Quigley, M., Krauss, Z., Lincoln, K., Attanayake, J., Stamp, L., Lanman, H., Levine, S., Hampton, S., and Gravley,
899 D.: Geologic and geomorphic controls on rockfall hazard: how well do past rockfalls predict future distributions?, Natural
900 Hazards and Earth System Sciences, 19, 2249–2280, https://doi.org/10.5194/nhess-19-2249-2019, 2019.

901 Bovis, M. J. and Evans, S. G.: Extensive deformations of rock slopes in southern Coast Mountains, southwest British
902 Columbia, Canada, Engineering Geology, 44, 163–182, https://doi.org/10.1016/S0013-7952(96)00068-3, 1996.

903 Brennan, K. and Whistler, R.: Railroad dock landslide, initial site visit trip report, Skagway, Alaska,
904 Geotechnical/Environmental Report, No. 109508-001, Shannon & Wilson, Anchorage, AK, USA, 2022.

905 Burns, W. J. and Madin, I. P.: Protocol for Inventory Mapping of Landslide Deposits from Light Detection and Ranging (lidar)
906 Imagery, Oregon Department of Geology and Mineral Industries (DOGAMI) Special Paper 42, 36p., 2009.

907 Callahan and Wayland: Geologic reconnaissance of the West Creek damsite near Skagway, Alaska, Geological Survey
908 Bulletin, 1211-A, https://doi.org/10.3133/b1211A, 1965.

909 Caviezel, A., Ringenbach, A., Demmel, S. E., Dinneen, C. E., Krebs, N., Bühler, Y., Christen, M., Meyrat, G., Stoffel, A.,
910 Hafner, E., Eberhard, L. A., Rickenbach, D. von, Simmler, K., Mayer, P., Niklaus, P. S., Birchler, T., Aebi, T., Cavigelli, L.,
911 Schaffner, M., Rickli, S., Schnetzler, C., Magno, M., Benini, L., and Bartelt, P.: The relevance of rock shape over mass—
912 implications for rockfall hazard assessments, Nat Commun, 12, 5546, https://doi.org/10.1038/s41467-021-25794-y, 2021.

913 Choi, M., Eaton, D. W., and Enkelmann, E.: Is the Eastern Denali fault still active?, Geology, 49, 662–666,
914 https://doi.org/10.1130/G48461.1, 2021.

915 Collins, B. D. and Stock, G. M.: Rockfall triggering by cyclic thermal stressing of exfoliation fractures, Nature Geoscience, 9,
916 395–400, https://doi.org/10.1038/ngeo2686, 2016.

917 Corominas, J., van Westen, C., Frattini, P., Cascini, L., Malet, J.-P., Fotopoulou, S., Catani, F., Van Den Eeckhaut, M.,
918 Mavrouli, O., Agliardi, F., Pitilakis, K., Winter, M. G., Pastor, M., Ferlisi, S., Tofani, V., Hervás, J., and Smith, J. T.:
919 Recommendations for the quantitative analysis of landslide risk, Bull Eng Geol Environ, 73, 209–263,
920 https://doi.org/10.1007/s10064-013-0538-8, 2014.

Cruden, D. M.: Limits to common toppling, Can. Geotech. J., 26, 737–742, https://doi.org/10.1139/t89-085, 1989.

Daly, C., Smith, J., and Halbleib, M.: 1981-2010 High-Resolution Temperature and Precipitation Maps for Alaska Final Report, Oregon State University, Corvallis, Oregon, 2018.

DGGS Staff: LiDAR Datasets of Alaska, Alaska Division of Geological & Geophysical Surveys, https://doi.org/10.14509/25239, 2013.

Dorren, L., Berger, F., Jonsson, M., Krautblatter, M., Mölk, M., Stoffel, M., and Wehrli, A.: State of the art in rockfall – forest interactions, Schweizerische Zeitschrift fur Forstwesen, 158, 128–141, https://doi.org/10.3188/szf.2007.0128, 2007.

Draebing, D., Mayer, T., Jacobs, B., and McColl, S. T.: Alpine rockwall erosion patterns follow elevation-dependent climate trajectories, Commun Earth Environ, 3, 1–12, https://doi.org/10.1038/s43247-022-00348-2, 2022.

Fanos, A. and Pradhan, B.: Laser Scanning Systems and Techniques in Rockfall Source Identification and Risk Assessment: A Critical Review, Earth Systems and Environment, 2, https://doi.org/10.1007/s41748-018-0046-x, 2018.

Frattini, P., Crosta, G., Carrara, A., and Agliardi, F.: Assessment of rockfall susceptibility by integrating statistical and physically-based approaches, Geomorphology, 94, 419–437, https://doi.org/10.1016/j.geomorph.2006.10.037, 2008.

Gigli, G., Lombardi, L., Carlà, T., Beni, T., and Casagli, N.: A method for full three-dimensional kinematic analysis of steep rock walls based on high-resolution point cloud data, International Journal of Rock Mechanics and Mining Sciences, 157, 105178, https://doi.org/10.1016/j.ijrmms.2022.105178, 2022.

Grant, A., Wartman, J., and Abou-Jaoude, G.: Multimodal method for coseismic landslide hazard assessment, Engineering Geology, 212, 146–160, https://doi.org/10.1016/j.enggeo.2016.08.005, 2016.

Gruber, S., Hoelzle, M., and Haeberli, W.: Permafrost thaw and destabilization of Alpine rock walls in the hot summer of 2003, Geophysical Research Letters, 31, https://doi.org/10.1029/2004GL020051, 2004.

Guerriero, L., Annibali Corona, M., Di Martire, D., Francioni, M., Limongiello, M., Tufano, R., and Calcaterra, D.: Rockfall susceptibility analysis of the "San Michele Arcangelo" historic trail (Central Italy) based on virtual outcrops and multiple propagation models, Bull Eng Geol Environ, 83, 263, https://doi.org/10.1007/s10064-024-03764-0, 2024.

Günther, A.: SLOPEMAP: programs for automated mapping of geometrical and kinematical properties of hard rock hill slopes, Computers & Geosciences, 29, 865–875, https://doi.org/10.1016/S0098-3004(03)00086-4, 2003.

Guzzetti, F., Reichenbach, P., and Wieczorek, G. F.: Rockfall hazard and risk assessment in the Yosemite Valley, California, USA, Natural Hazards and Earth System Sciences, 3, 491–503, https://doi.org/10.5194/nhess-3-491-2003, 2003.

Hales, T. C. and Roering, J. J.: Climatic controls on frost cracking and implications for the evolution of bedrock landscapes, Journal of Geophysical Research, 112, https://doi.org/10.1029/2006JF000616, 2007.

Harris, A. S. and Farr, W. A.: The forest ecosystem of southeast Alaska: 7. Forest ecology and timber management., Gen. Tech. Rep. PNW-GTR-025. Portland, OR: U.S. Department of Agriculture, Forest Service, Pacific Northwest Research Station. 116 p, 025, 1974.

Hooyer, T. S., Cohen, D., and Iverson, N. R.: Control of glacial quarrying by bedrock joints, Geomorphology, 153–154, 91–101, https://doi.org/10.1016/j.geomorph.2012.02.012, 2012.

Horel, J., Splitt, M., Dunn, L., Pechmann, J., White, B., Ciliberti, C., Lazarus, S., Slemmer, J., Zaff, D., and Burks, J.: MESOWEST: COOPERATIVE MESONETS IN THE WESTERN UNITED STATES, 2002.

Huggel, C., Allen, S., Deline, P., Fischer, L., Noetzli, J., and Ravanel, L.: Ice thawing, mountains falling—are alpine rock slope failures increasing?, Geology Today, 28, 98–104, https://doi.org/10.1111/j.1365-2451.2012.00836.x, 2012.

Hungr, O., Evans, S. G., and Hazzard, J.: Magnitude and frequency of rock falls and rock slides along the main transportation corridors of southwestern British Columbia, Can. Geotech. J., 36, 224–238, https://doi.org/10.1139/t98-106, 1999.

Hungr, O., Leroueil, S., and Picarelli, L.: The Varnes classification of landslide types, an update, Landslides, 11, 167–194, https://doi.org/10.1007/s10346-013-0436-y, 2014.

Imaizumi, F., Nishii, R., Murakami, W., and Daimaru, H.: Parallel retreat of rock slopes underlain by alternation of strata, Geomorphology, 238, 27–36, https://doi.org/10.1016/j.geomorph.2015.02.030, 2015.

Kleinn, J., Christen, M., and Bartelt, P.: Probabilistic event-based rockfall modelling for deriving continuous intensity-frequency curves in the impact area, Interpraevent 2024. Conference proceedings, 648–652, 2024.

Klimeš, J., Kilnar, J., Kopačková-Strnadová, V., Pánek, T., McColl, S., and Jelének, J.: Landslides in the glaciated mountains of the Cordillera Blanca, Peru—types, spatial distribution, and conditioning factors, Landslides, https://doi.org/10.1007/s10346-024-02387-6, 2024.

Krabbendam, M. and Glasser, N. F.: Glacial erosion and bedrock properties in NW Scotland: Abrasion and plucking, hardness and joint spacing, Geomorphology, 130, 374–383, https://doi.org/10.1016/j.geomorph.2011.04.022, 2011.

Krautblatter, M., Funk, D., and Günzel, F. K.: Why permafrost rocks become unstable: a rock–ice-mechanical model in time and space, Earth Surface Processes and Landforms, 38, 876–887, https://doi.org/10.1002/esp.3374, 2013.

Kundu, J., Sarkar, K., Ghaderpour, E., Mugnozza, G. S., and Mazzanti, P.: A GIS-Based Kinematic Analysis for Jointed Rock Slope Stability: An Application to Himalayan Slopes, Land, 12, https://doi.org/10.3390/land12020402, 2023.

LaHusen, S. R., Duvall, A. R., Booth, A. M., Grant, A., Mishkin, B. A., Montgomery, D. R., Struble, W., Roering, J. J., and Wartman, J.: Rainfall triggers more deep-seated landslides than Cascadia earthquakes in the Oregon Coast Range, USA, Science Advances, 6, eaba6790, https://doi.org/10.1126/sciadv.aba6790, 2020.

Leine, R. I., Schweizer, A., Christen, M., Glover, J., Bartelt, P., and Gerber, W.: Simulation of rockfall trajectories with consideration of rock shape, Multibody Syst Dyn, 32, 241–271, https://doi.org/10.1007/s11044-013-9393-4, 2014.

Leith, K., Moore, J. R., Amann, F., and Loew, S.: In situ stress control on microcrack generation and macroscopic extensional fracture in exhuming bedrock: FRACTURE GENERATION IN EXHUMING BEDROCK, Journal of Geophysical Research: Solid Earth, 119, 594–615, https://doi.org/10.1002/2012JB009801, 2014.

Loye, A., Jaboyedoff, M., and Pedrazzini, A.: Identification of potential rockfall source areas at a regional scale using a DEM-based geomorphometric analysis, Nat. Hazards Earth Syst. Sci., 9, 1643–1653, https://doi.org/10.5194/nhess-9-1643-2009, 2009.

Lu, G., Caviezel, A., Christen, M., Demmel, S. E., Ringenbach, A., Bühler, Y., Dinneen, C. E., Gerber, W., and Bartelt, P.: Modelling rockfall impact with scarring in compactable soils, Landslides, 16, 2353–2367, https://doi.org/10.1007/s10346-019-01238-z, 2019.

Lu, G., Ringenbach, A., Caviezel, A., Sanchez, M., Christen, M., and Bartelt, P.: Mitigation effects of trees on rockfall hazards: does rock shape matter?, Landslides, 18, 59–77, https://doi.org/10.1007/s10346-020-01418-2, 2021.

Luckman, B. H.: Rockfalls and rockfall inventory data: Some observations from surprise valley, Jasper National Park, Canada, Earth Surface Processes, 1, 287–298, https://doi.org/10.1002/esp.3290010309, 1976.

Macpherson, A. E., Nicolsky, D. J., and Suleimani, E. N.: Digital elevation models of Skagway and Haines, Alaska: Procedures, data sources, and quality assessment, Alaska Division of Geological & Geophysical Surveys, https://doi.org/10.14509/29143, 2014.

Marquínez, J., Menéndez Duarte, R., Farias, P., and JiméNez Sánchez, M.: Predictive GIS-Based Model of Rockfall Activity in Mountain Cliffs, Natural Hazards, 30, 341–360, https://doi.org/10.1023/B:NHAZ.0000007170.21649.e1, 2003.

Matasci, B., Stock, G. M., Jaboyedoff, M., Carrea, D., Collins, B. D., Guérin, A., Matasci, G., and Ravanel, L.: Assessing rockfall susceptibility in steep and overhanging slopes using three-dimensional analysis of failure mechanisms, Landslides, 15, 859–878, https://doi.org/10.1007/s10346-017-0911-y, 2018.

Matsuoka, N. and Sakai, H.: Rockfall activity from an alpine cliff during thawing periods, Geomorphology, 28, 309–328, https://doi.org/10.1016/S0169-555X(98)00116-0, 1999.

Mayer, T., Deprez, M., Schröer, L., Cnudde, V., and Draebing, D.: Quantifying frost-weathering-induced damage in alpine rocks, The Cryosphere, 18, 2847–2864, https://doi.org/10.5194/tc-18-2847-2024, 2024.

Meentemeyer, R. K. and Moody, A.: Automated mapping of conformity between topographic and geological surfaces, Computers & Geosciences, 26, 815–829, https://doi.org/10.1016/S0098-3004(00)00011-X, 2000.

Menounos, B., Goehring, B. M., Osborn, G., Margold, M., Ward, B., Bond, J., Clarke, G. K. C., Clague, J. J., Lakeman, T., Koch, J., Caffee, M. W., Gosse, J., Stroeven, A. P., Seguinot, J., and Heyman, J.: Cordilleran Ice Sheet mass loss preceded climate reversals near the Pleistocene Termination, Science, 358, 781–784, https://doi.org/10.1126/science.aan3001, 2017.

Messenzehl, K., Meyer, H., Otto, J.-C., Hoffmann, T., and Dikau, R.: Regional-scale controls on the spatial activity of rockfalls (Turtmann Valley, Swiss Alps) — A multivariate modeling approach, Geomorphology, 287, 29–45, https://doi.org/10.1016/j.geomorph.2016.01.008, 2017.

Michoud, C., Derron, M.-H., Horton, P., Jaboyedoff, M., Baillifard, F.-J., Loye, A., Nicolet, P., Pedrazzini, A., and Queyrel, A.: Rockfall hazard and risk assessments along roads at a regional scale: example in Swiss Alps, Natural Hazards and Earth System Sciences, 12, 615–629, https://doi.org/10.5194/nhess-12-615-2012, 2012.

Moore, J. R., Sanders, J. W., Dietrich, W. E., and Glaser, S. D.: Influence of rock mass strength on the erosion rate of alpine cliffs, Earth Surface Processes and Landforms, 34, 1339–1352, https://doi.org/10.1002/esp.1821, 2009.

Moos, C., Khelidj, N., Guisan, A., Lischke, H., and Randin, C. F.: A quantitative assessment of rockfall influence on forest structure in the Swiss Alps, Eur J Forest Res, 140, 91–104, https://doi.org/10.1007/s10342-020-01317-0, 2021.

Munson, M.: Railroad Dock landslides continue, declaration of emergency in place, The Skagway News, 12th August, 2022a.

Munson, M.: Rockslide at cruise ship dock – Skagway's Railroad Dock has limited use, The Skagway News, 23rd June, 2022b.

Nash, D., Rutz, J. J., and Jacobs, A.: Atmospheric Rivers in Southeast Alaska: Meteorological Conditions Associated With Extreme Precipitation, Journal of Geophysical Research: Atmospheres, 129, e2023JD039294, https://doi.org/10.1029/2023JD039294, 2024.

Oliinyk, M., Bubniak, I., and Vikhot, Y.: Using Move software by geological field works, International Conference of Young Professionals «GeoTerrace-2020», 1–5, https://doi.org/10.3997/2214-4609.20205706, 2020.

Paranunzio, R., Laio, F., Nigrelli, G., and Chiarle, M.: A method to reveal climatic variables triggering slope failures at high elevation, Nat Hazards, 76, 1039–1061, https://doi.org/10.1007/s11069-014-1532-6, 2015.

Paranunzio, R., Laio, F., Chiarle, M., Nigrelli, G., and Guzzetti, F.: Climate anomalies associated with the occurrence of rockfalls at high-elevation in the Italian Alps, Natural Hazards and Earth System Sciences, 16, 2085–2106, https://doi.org/10.5194/nhess-16-2085-2016, 2016.

Pawlik, Ł., Phillips, J. D., and Šamonil, P.: Roots, rock, and regolith: Biomechanical and biochemical weathering by trees and its impact on hillslopes—A critical literature review, Earth-Science Reviews, 159, 142–159, https://doi.org/10.1016/j.earscirev.2016.06.002, 2016.

Poage, N. J., Marshall, D. D., and McClellan, M. H.: Maximum Stand-Density Index of 40 Western Hemlock–Sitka Spruce Stands in Southeast Alaska, Western Journal of Applied Forestry, 22, 99–104, https://doi.org/10.1093/wjaf/22.2.99, 2007.

Priest, S. D. and Hudson, J. A.: Estimation of discontinuity spacing and trace length using scanline surveys, International Journal of Rock Mechanics and Mining Sciences & Geomechanics Abstracts, 18, 183–197, https://doi.org/10.1016/0148-9062(81)90973-6, 1981.

Rapp, A.: Talus slopes and mountain walls at Tempelfjorden, Spitsbergen : a geomorphological study of the denudation of slopes in an Arctic locality, Skritfter, Norsk Polarinstitutt, 119, 1960.

Ravanel, L., Deline, P., Lambiel, C., and Vincent, C.: Instability of a High Alpine Rock Ridge: the Lower Arête Des Cosmiques, Mont Blanc Massif, France, Geografiska Annaler: Series A, Physical Geography, 95, 51–66, https://doi.org/10.1111/geoa.12000, 2013.

Rempel, A. W., Marshall, J. A., and Roering, J. J.: Modeling relative frost weathering rates at geomorphic scales, Earth and Planetary Science Letters, 453, 87–95, https://doi.org/10.1016/j.epsl.2016.08.019, 2016.

Ringenbach, A., Bebi, P., Bartelt, P., Rigling, A., Christen, M., Bühler, Y., Stoffel, A., and Caviezel, A.: Shape still matters: rockfall interactions with trees and deadwood in a mountain forest uncover a new facet of rock shape dependency, Earth Surface Dynamics, 11, 779–801, https://doi.org/10.5194/esurf-11-779-2023, 2023.

Roering, J. J., Dedinsky, K., Grilliot, M., Wachino, I. D., and Cash, R.: Skagway Landslide Hazard, RAPID Facility, https://doi.org/doi.org/10.17603/ds2-2e3p-yn12, 2025.

Rosser, N. and Massey, C.: Rockfall hazard and risk, in: Landslide Hazards, Risks, and Disasters, Elsevier, 581–622, https://doi.org/10.1016/B978-0-12-818464-6.00013-5, 2022.

Rosser, N., Lim, M., Petley, D., Dunning, S., and Allison, R.: Patterns of precursory rockfall prior to slope failure, Journal of Geophysical Research: Earth Surface, 112, https://doi.org/10.1029/2006JF000642, 2007.

Royán, M. J., Abellán, A., Jaboyedoff, M., Vilaplana, J. M., and Calvet, J.: Spatio-temporal analysis of rockfall pre-failure deformation using Terrestrial LiDAR, Landslides, 11, 697–709, https://doi.org/10.1007/s10346-013-0442-0, 2014.

Ruffner, C. M. and Abrams, M. D.: Relating land-use history and climate to the dendroecology of a 326-year-old Quercus prinus talus slope forest, Can. J. For. Res., 28, 347–358, https://doi.org/10.1139/x97-220, 1998.

Samodra, G., Chen, G., Sartohadi, J., Hadmoko, D. S., Kasama, K., and Setiawan, M. A.: Rockfall susceptibility zoning based on back analysis of rockfall deposit inventory in Gunung Kelir, Java, Landslides, 13, 805–819, https://doi.org/10.1007/s10346-016-0713-7, 2016.

Sarro, R., Rossi, M., Reichenbach, P., and Mateos, R. M.: From rockfall source areas identification to susceptibility zonation: a proposed workflow tested in El Hierro (Canary Islands, Spain), Natural Hazards and Earth System Sciences Discussions, 1–30, https://doi.org/10.5194/nhess-2024-85, 2024.

Scheidl, C., Heiser, M., Vospernik, S., Lauss, E., Perzl, F., Kofler, A., Kleemayr, K., Bettella, F., Lingua, E., Garbarino, M., Skudnik, M., Trappmann, D., and Berger, F.: Assessing the protective role of alpine forests against rockfall at regional scale, Eur J Forest Res, 139, 969–980, https://doi.org/10.1007/s10342-020-01299-z, 2020.

Statham, I.: A scree slope rockfall model, Earth Surface Processes, 1, 43–62, https://doi.org/10.1002/esp.3290010106, 1976.

van Steijn, H.: Long-term landform evolution: evidence from talus studies, Earth Surface Processes and Landforms, 27, 1189–1199, https://doi.org/10.1002/esp.420, 2002.

Stock, G. M. and Collins, B. D.: Quantitative Rockfall hazard and risk assessment for Yosemite Valley, Yosemite National Park, California, USGS Scientific Investigations Report 2014-5129, 2014.

Stock, G. M., Bawden, G. W., Green, J. K., Hanson, E., Downing, G., Collins, B. D., Bond, S., and Leslar, M.: High-resolution three-dimensional imaging and analysis of rock falls in Yosemite Valley, California, Geosphere, 7, 573–581, https://doi.org/10.1130/GES00617.1, 2011.

Stoffel, M., Lièvre, I., and Monbaron, M.: Seasonal timing of rockfall activity on a forested slope at Täschgufer (Swiss Alps) - a dendrochronological approach, Zeitschrift für Geomorphologie, 89–106, 2005.

Stoffel, M., Trappmann, D. G., Coullie, M. I., Ballesteros Cánovas, J. A., and Corona, C.: Rockfall from an increasingly unstable mountain slope driven by climate warming, Nat. Geosci., 1–6, https://doi.org/10.1038/s41561-024-01390-9, 2024.

Terzaghi, R. D.: Sources of Error in Joint Surveys, Géotechnique, 15, 287–304, https://doi.org/10.1680/geot.1965.15.3.287, 1965.

The Daily Alaskan: SLIDE: Hill again caves in near Moore's Wharf, The Daily Alaskan, 20th October, 1, 1901.

Thompson, P.: Alaska Department of Transportation & Public Facilities (AKDOT) Geotechnical Asset Management Program, Technical Report STP000S(802)(B), Juneau, AK, 2017.

Thornton, T. F.: Our Grandparents' Names on the Land/Haa Leelk'w Has Aani Saax'u, University of Washington Press, Seattle, WA, 256 pp., 2010.

Utlu, M., Öztürk, M. Z., Şimşek, M., and Akgümüş, M. F.: Evaluation of rockfall hazard based on UAV technology and 3D Rockfall Simulations, International Journal of Environment and Geoinformatics, 10, 1–16, https://doi.org/doi.%252010.30897/ijegeo.10323768, 2023.

Western Regional Climate Center: https://wrcc.dri.edu, last access: 14 August 2025.

Whalley, B.: Rockfalls, in: Slope Instability, Wiley, Chichester, UK, 217–256, 1984.

Wieczorek, G. F. and Jäger, S.: Triggering mechanisms and depositional rates of postglacial slope-movement processes in the Yosemite Valley, California, Geomorphology, 15, 17–31, https://doi.org/10.1016/0169-555X(95)00112-I, 1996.

Wright, B. E., Plumb, P., Wright, J., and Biles, F. E.: Historical photographs from U.S. Forest Service research and development activities in Alaska, https://doi.org/10.2737/RDS-2021-0084, 2021.

Wyllie, D. C. and Mah, C. W.: Rock Slope Engineering, 4th ed., Spon, 456 pp., 2004.

Yehle, L. A. and Lemke, R. W.: Reconnaissance engineering geology of the Skagway area, Alaska with emphasis on evaluation of earthquake and other geologic hazards, USGS Open File Report, 1972.